Analyses of Thin Films and Solid-Liquid Interfaces Using Picosecond Transient Reflecting Grating (TRG) Technique

（ピコ秒過渡反射格子法を用いた薄膜や固液界面の分析）

Qing Shen

Analyses of Thin Films and Solid-Liquid Interfaces Using Picosecond Transient Reflecting Grating (TRG) Technique

（ピコ秒過渡反射格子法を用いた薄膜や固液界面の分析）

by Qing Shen

Department of Applied Chemistry

Faculty of Engineering

University of Tokyo

January 1995

Supervisor: Professor Tsuguo Sawada

Preface

The present thesis collects studies carried out under the direction of Professor Tsuguo Sawada at the University of Tokyo during 1992-1995.

The studies are concerned with the *Analyses of Thin Films and Solid-Liquid Interfaces Using Picosecond Transient Reflecting Grating (TRG) Technique.* Their objectives were to explore and demonstrate, both theoretically and experimentally, the capabilities and potentials of the TRG technique in the research and characterization of ultrathin films and interfaces as a novel *in situ*, non-contact and non-destructive evaluation method. For example, the TRG technique can be used to evaluate the elastic properties of not only the surface layer, but also an intermediate layer of ultrathin (thicknesses: from a few dozen nm to a few hundred nm) multilayered films, the thermal properties of ultrathin films (thicknesses: a few dozen nm) such as diamondlike carbon films deposited on multilayered substrates, the properties of electrode/solution interfaces *in situ*, and so on. These properties are of a great importance in technology and science, but they are impossible or rather difficult to detect *in situ*, by a non-contact and non-destructive method based on conventional means.

This thesis is organized into six chapters which can be summarized as follows.

Chapter 1 is a general introduction. It presents the background and objectives of these studies, including the historical development of the TRG technique and comparison of its distinctive features with other methods.

Chapter 2 describes the principle and experimental arrangement of the TRG technique.

Chapter 3 proves the capabilities and potentials of the TRG technique to investigate the elastic and thermal properties of ultrathin films (thickness: a few dozen nm) deposited on multilayered substrates. As an example, nonimplanted and ion-implanted diamondlike carbon films 40 nm in thickness were studied with the TRG technique.

Chapter 4 establishes a novel method, theoretically and experimentally, to evaluate the elastic properties of an intermediate layer besides the surface layer for ultrathin multilayered films using the TRG technique. The capabilities of this method were demonstrated by measuring the acoustic velocities of the Au layer (thickness: 300nm) and the Cr layer (thickness: 30nm) for a Au/Cr/quartz sample. This method was also applied to determine the thicknesses of thin Au films deposited on soda lime glass substrates.

Chapter 5 discusses the abilities and potentials of the TRG technique to study the properties of liquid/solid interfaces *in situ* such as electrode/solution interfaces,

but especially for the interfaces of liquid/film/substrate systems. In this chapter, a general theory is developed to analyze the TRG signals at interfaces (e. g., gas/solid, liquid/solid), with which some experimental results are explained very well. For the first time, it is established dtheoretically and experimentally that longitudinal acoustic pulses (frequency: from a few dozen GHz to a few hundred GHz) normal to the sample surface could be generated and detected at the surfaces of thin films by the TRG technique. It is proposed that the TRG technique is applicable to characterization of electrochemical interfaces *in situ*. For example, it can be used to monitor the changes in the properties of electric double layers versus electrode potentials.

Chapter 6 gives some concluding remarks and perspectives on the TRG technique.

Qing Shen

January 1995

CONTENTS

CHAPTER 1

Introduction

1.1 Background

Over the past few decades, there has been heightened interest in the development and application of *in situ* techniques for investigating the properties of ultrathin films or interfaces (such as gas/solid, solid/liquid and solid/solid interfaces) in a non-contact, non-destructive fashion. This is because of the expanding and important roles that ultrathin films or interfaces play in fields like microelectronics, optics, and biomedical industries. As examples(Fig. 1.1), attempts are being made to use diamond or diamondlike carbon films with thicknesses of a few dozen nm as protective overcoats for magnetic and optical recording disks; thin metallic intermediate layers, a few dozen nm thick, are deposited between metallic surface layers and substrates to improve their adhesion; and electrode/electrolyte solution interfaces (electrical double layers) are scientifically and technologically important in a wide variety of physicochemical processes. As a result, *in situ* measurements of the thermal and elastic properties of thin regions at sample surfaces or

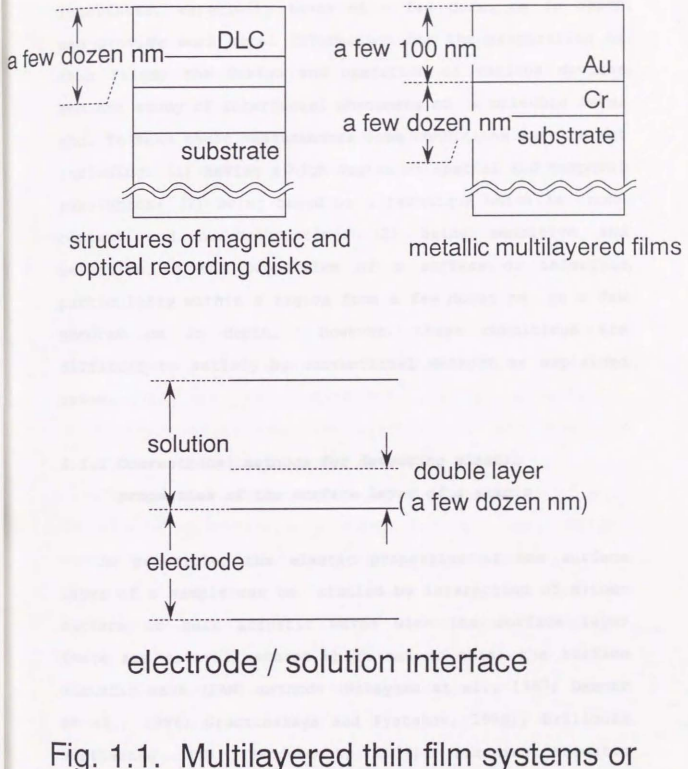

Fig. 1.1. Multilayered thin film systems or electrode / solution interface.

interfaces, especially those of a few dozen nm in depth, can provide much vital information for the preparation of thin films, the design and operation of various devices, and the study of interfacial phenomena on a molecule level etc. To make these measurements some conditions must be met including: (1) having a high degree of spatial and temporal resolution; (2) being based on a technique which is non-contact and non-destructive; (3) being sensitive and selective to the properties of a surface or interface, particularly within a region from a few dozen nm to a few hundred nm in depth. However, these conditions are difficult to satisfy by conventional methods as explained below.

1.1.1 Conventional methods for detecting elastic properties of the surface layer of a sample

In principle, the elastic properties of the surface layer of a sample can be studied by interaction of either surface or bulk acoustic waves with the surface layer. There are several methods which can do this: the surface acoustic wave (SAW) methods (Nakayama et al., 1987; Danner et al., 1986; Grudzinskaya and Pyatakov, 1989), Brillouin scattering (BS) (Sandercock, 1978), scanning acoustic microscopy (SAM) (Briggs, 1985; Kushibiki and Chubachi, 1985), and laser picosecond acoustics (Thomsen et al, 1986; Grahn et al, 1989; Wright et al, 1991; Clemens and Eesley,

1988) methods. Each of the techniques is sensitive to the acoustic properties of different depths in the sample close to the immediate vicinity of the surface. For SAW methods, elastic properties of a surface layer as thin as one tenths of the SAW wavelength can be evaluated.

For the conventional SAW method, a pair of interdigital transducers (IDTs) is deposited on a piezoelectric material to excite and detect the SAWs. Although sensitive, the resonant frequencies of the IDTs are generally a few 100 MHz, at which the SAW wavelengths are a few dozen μm. Thus this method is difficult to use to measure the elastic properties of thin films with thicknesses less than 100nm, especially when the substrates are non-piezoelectric. Furthermore mechanical and electric contact with the substrate is necessary.

The BS technique allows the elastic properties of small samples to be studied in a non-contact way, under various conditions e. g. low temperature, high pressure, or in a magnetic field etc. Surface phonons with high frequency range of GHz - 100 GHz can be excited and hence the elastic properties of thin films a few hundred nm thick can be studied. However, this technique requires the sample surface to be of very high optical quality. The experimental equipment must have high sensitivity and the measurement time is also long.

SAM is a powerful tool in the study of elastic properties of materials and in non-destructive examination.

SAM can excite SAWs with wavelengths on the order of 1 μm. However, in the measurement, samples must be in contact with the couplers such as water. Thus this method is not applicable for *in situ* study of elastic properties of samples in a non-contact way. For example, it is difficult to measure the samples which are placed in liquids.

Recently, a promising method has been developed for studying the elastic properties of thin films with laser picosecond acoustics using the optical pump-probe technique. Sound pulses of a duration of a few picoseconds can be generated, which propagate perpendicular to the sample surface and are reflected from the film/substrate and air/film interfaces. By detecting these sound pulses at the sample surface, this technique can be used to determine either the thickness or the sound velocity of opaque thin films in the 10-1000nm thickness range as a non-contact method. However, this method has poor sensitivity, and only longitudinal acoustic velocity of the thin film can be detected, so the information ia lacking about all of the elastic constants of the film.

1.1.2 Conventional methods for detecting the thermal properties of the surface layer of a sample

The traditional methods (Hirschman et al., 1961) using

thermocouples in contact with a sample are not applicable when measuring the thermal property of a thin surface layer of a sample. This is because the contribution of the thermal property for the thin surface layer to that of the combined film/substrate system determined by these methods is too small to be extracted. It is of course undesirable to lift the surface layer from the substrate, because not only is this destructive, but it also misses *in situ* thermal property having coupling to the substrate. Recently, Griffin et al. (1994) reported their results the transverse thermal diffusivity of thin dielectric films with thicknesses of less than a few dozen nm. However, metallic stripes and contact pads must be deposited on the sample surface and hence the sample size must be large enough.

Several photothermal (PT) techniques such as thermal wave mirage effect, photothermal displacement and thermoreflectance measurements have been applied successfully to study the thermal property of samples as *in situ*, non-contact and non-destructive methods. In all of these methods, thermal waves are generated at the sample surfaces by periodic or pulsed, focused laser beams. Then the thermal properties of the samples can be evaluated by measuring the corresponding temperature field in the surrounding area with the mirage technique (Jackson et al., 1981; Lai et al., 1982; Petzoldt et al., 1988; Kuo et al., 1989), photothermal surface displacement signals (Olmstead

et al., 1983; Welsch et al., 1990; Karner et al., 1985), or the photothermal reflection signals (Rosencwaig et al., 1985). The principles of all these methods are based on photothermal processes, and hence the measured thermal property is sensitive to the depth of thermal diffusion length, which is larger than 1 μm, in general, because of the restriction of the experimental conditions. So they are not easily used to study the thermal properties of a thin surface layer less than 100 nm in depth in a sample.

On the basis of the above background, it becomes apparent that a novel, sensitive, non-contact, and non-destructive method should be developed for investigating physical properties such as the thermal and elastic properties of a thin surface layer less than 100nm in depth. In this thesis, a method which has good capabilities and potentials for research and characterization of surfaces and interfaces, has been studied and developed. It is the transient reflecting grating (TRG) technique, which is one kind of laser-induced grating (LIG) technique (Eichler et al., 1986; Harata, 1990). In the following, a brief historical overview of LIG and TRG techniques is given.

1.1.3 Laser-induced grating (LIG) technique

The LIG technique generates and detects dynamic or transient gratings induced by laser beams. In the LIG technique, two time-coincident laser pulses of the same

frequency are crossed on a sample to form an optical interference pattern. Light absorption results in a spatially periodic sinusoidal distribution of excited states. Since the optical properties of the excited states differ from those of the ground states, the excited state concentration distribution acts as a transient diffraction grating, which is known as an "excited state grating" (Nelson et al., 1982). On the other hand, if absorption of the excitation pulses is followed by rapid radiationless relaxation, a spatially periodic temperature distribution is generated and the subsequent thermal expansion launches counter-propagating acoustic waves. Since the optical properties of a system are density dependent, a transient diffraction grating is created which can be considered to be formed by thermal and acoustic gratings (Eichler et al., 1986). In this thesis, the main interest has been the latter. After the excitation pulses disappear, the transient gratings (TGs) will decay with time because of thermal diffusion, acoustic oscillations or other dynamic relaxations. Thus by measuring the TG responses, properties, such as thermal and acoustic properties, of the sample in the region of the gratings can be monitored.

The LIG experiments were first done in the 1960's along with the development of various laser systems with sufficient power (Bboersch and Eichler, 1967; Eichler, 1986). Then during the late 1960's and 1970's a large body of research was produced in the stimulated scattering

processes by dynamic gratings, such as stimulated thermal scattering (STS) (Pohl et al., 1968a and 1969 b; Pohl, 1969), stimulated Brillouin Scattering (SBS) (Denariez and Ret, 1968; Pohl et al., 1968a and 1968b; Pohl et al., 1969), stimulated thermal Brillouin Scattering (STBS) (Pohl et al., 1968a), stimulated Rayleigh wing scattering (SRWS) (Denariez and Ret, 1968), and stimulated Raman scattering (SRS) (Bloembergen et al., 1967). Eichler et al. (1973) used the LIGs to determine heat diffusivities in ruby and glycerol. They also studied the excitation of sound waves in an absorbing sample by modulated light beams derived from a mode-locked ruby laser (Eichler and Stahl, 1973).

Phillion et al. (1975) developed a novel transient grating (TG) method by introducing an optical pump-probe into the LIG experiment. Most significantly, they improved time resolution up to about the laser pulsewidth by diffracting the variable-delay laser probe pulse by the LIGs. Their method can be applied to measure a variety of atomic and molecular excited state phenomena on subnanosecond to picosecond time scales. Various applications of the LIG technique have been proposed. One was the picosecond holographic grating generating of ultrasonics (Nelson et al., 1982; Fayer, 1986; Yan et al., 1988; Harata et al., 1987; Harata and Sawada, 1988). Another application was laser-induced phonon spectroscopy (LIPS) technique (Fayer, 1986), which was used to measure a variety of physical properties of systems in condensed

phases, such as a very weak ground absorption (Miller et al., 1982), an excited state-excited state absorption (Miller et al., 1984), optoelastic constants, elasticity parameters, and acoustic attenuation (Miller et al., 1982), the anisotropic elasticity (Nelson et al., 1982), ect.

In all of the experiments mentioned above, the LIGs were induced in the bulk of the samples to study the bulk properties. In contrast with this, the LIGs can also be induced on sample surfaces to generate SAWs and study the properties of sample surfaces. The idea of excitation of SAWs by LIGs was first proposed by Auth (1970), while Cachier (1970) attempted it in an experiment. Almost two decades later, Kasinski et al. (1988) published experimental results for generation of SAWs on transparent semiconductor (TiO_2) surfaces. Later, Harata et al. (1990) successfully generated and detected SAWs on the surfaces of opaque samples like an aluminum film and a silicon single crystal. They used the transient reflecting grating (TRG) method for the first time.

1.1.4 Transient reflecting grating (TRG) technique

The LIG technique ia actually of two types, the transient reflecting grating (TRG) technique and the transient transmitting grating (TTG) technique. The former diffracts the probe beam in a reflected geometry, while the latter diffracts in a transmitted geometry. The TTG

technique has larger diffraction efficiency than the TRG method, but it is not applicable to opaque samples. The TTG diffraction signals primarily measure the mean bulk properties of the sample (Fishman et al., 1993). In contrast with this, the TRG technique is very sensitive and selective to the surface and interface properties (Fishman et al., 1993; Harata et al., 1990). The TRG technique is a promising tool for studying not only the elastic but also the thermal properties at the same time of either bulk material or thin films, and it has many advantages over other methods as summarized in Table 1.1. For example, the TRG technique is non-contact, non-destructive, *in situ*, and has an excellent capability for generating and detecting high-power coherent ultrasonic waves of a few megahertz to 30GHz. The TRG technique has a high degree of temporal resolution up to a pulse width of a few dozen ps by using the synchronously delayed optical pump-probe method. It can be used to study ultrafast photothermal (PT) and photoacoustic (PA) phenomena. It also has a higher degree of spatial resolution than the conventional PT and PA methods (Harata et al., 1995).

To the author's knowledge, Harata et al. (1990) were the first to study acoustic and thermal properties of opaque samples using TRGs. This group, at the University of Tokyo under the direction of Prof. Sawada, applied the TRG method to evaluate the changes of physical properties, such as thermal diffusivity, SAW velocity and Auger

Table 1.1 Methods for measuring optical, thermal and acoustic properties of surface or interface.

Methods	measurable physical property			non-contact	measurable depth
	optical	thermal	acoustic		
conventional SAW methods	×	×	○	×	a few μm - a few mm
scanning acoustic microscopy	×	×	○	×	1mm - a few mm
photothermal/ photoacoustic method	○	○	×	△	1mm - a few mm
transient reflecting grating method	○	○	○	○	a few dozen nm - a few mm

recombination rate, on an ion implanted silicon surface due to ion implantation (Harata et al., 1990; Harata and Sawada, 1991; Harata et al., 1993a and 1993b; Nishimura et al., 1993). This group has also used the TRG method to study electrochemical interfaces (Harata, 1992; Harata et al., 1995).

Other researchers have also shown interest in studying the thermal and acoustic properties of sample surfaces or thin films by the TRG technique. Impulsive stimulated thermal scattering (ISTS) method, which uses the same principle as the TRG method, has been used to study acoustic properties of supported and unsupported polyimide thin films of about 1μm thickness (Duggal et al., 1992a and 1992b; Rogers and Nelson, 1994; Rogers et al., 1994). The TRG technique has been used to measure thermal diffusivities of polycrys-talline copper and nickel, and diamond thin films (Jauregui and Matthias, 1992; Käding et al., 1993). In these experiments, the grating spacings varied from a few dozen μm to a few 100 μm and the thicknesses of the thin films measured were a few μm.

Besides the above experimental works, several theoretical studies have also appeared. Theoretical calculation methods were given to obtain analytical solutions for excitation of pseudo-Rayleigh acoustic modes and the waveguide acoustic modes, and to extract the elastic properties of thin films from the solutions (Duggal et al., 1992b; Rogers and Nelson, 1994). However, only a

single-layer film/substrate system model was considered in these analyses and it is not applicable to multilayered film/substrate systems. Kasinski et al. (1988) have interpreted their experimental results on SAWs induced by TGs, theoretically. However, they made an approximation that the time scale for thermal diffusion was much longer than the experimental time scale which is not valid for those materials with large thermal diffusivities like metals. Fishman et al. (1993) have developed a general theory for transient grating diffraction from both sides of a single interface. But they only considered the optical diffraction process in detail, and did not give solutions of temperature and acoustic modes induced by the TGs which are important for analysis of TRG signals and waveforms.

As outlined above, a general theory for extracting the exact, analytical solutions for both the temperature and acoustic fields induced by TGs remains to be developed. Such a theory is very important for explaining experimental results (Harata, 1992; Harata et al., 1995), and for extracting the thermal and elastic properties of sample surfaces or interfaces.

1.2 Objectives

As demonstrated above, the TRG technique has proved to be a remarkable tool for studying thermal and acoustic properties of either bulk and thin films as a sensitive, *in situ*, non-contact, and non-destructive evaluation method.

However, to the author's knowledge, the TRG technique has not been applied to studies of films thinner than 100nm or to multilayered films, and a general theory for analyzing the thermal and acoustic gratings as well as the TRG signals also remained to be established.

Then, the first objective of this study is to explore and demonstrate the capabilities and potentials of the TRG technique in research and experimental characterization of thin films of less than 100nm thickness and multilayered films. A method is presented for detecting the elastic properties (not only the transverse, but also the vertical sound velocities) of both the surface layer and intermediate layer of ultrathin multilayered films (thicknesses: from a few dozen nm to a few 100 nm). The second objective is to develop a general theory for analyzing the TRG signals on sample surfaces and interfaces (e. g., liquid/solid and gas/solid interfaces), in which both the transient temperature and the acoustic displacement fields are taken into consideration. On the basis of the theory, some experimental results such as those on the electrochemical interfaces given by Harata et al. (1995) are analyzed. For the first time , it is seen that longitudinal acoustic pulses (frequency: from a few dozen GHz to a few 100 GHz) normal to the sample surface can be generated and detected at the surfaces of thin films by the TRG technique.

CHAPTER 2

Principle and experimental arrangement of the TRG technique

In this chapter, the principle of excitation and detection of TGs and the experimental arrangement of the TRG technique are described. The TRGs are excited by interference of two laser beams and the following rapid nonradiative relaxation processes. They are detected by diffraction of a probe beam. An optical pump-probe technique is introduced into the experimental arrangement which improves the temporal resolution up to a few dozen ps.

2.1 Principle

2.1.1 Excitation of the TGs

The principle of excitation of TGs is schematically shown in Fig. 2.1 (a). When two time-coincident short laser pulses (excitation beams) with the same wavelength λ and intensity I intersect at an angle 2θ at the sample surface or interface, an optical interference pattern with a grating spacing Λ can be created, which is called an interference grating (Eichler et al., 1986). The direction of the grating vector is taken as the x direction. The grating spacing Λ is tunable by changing the crossing

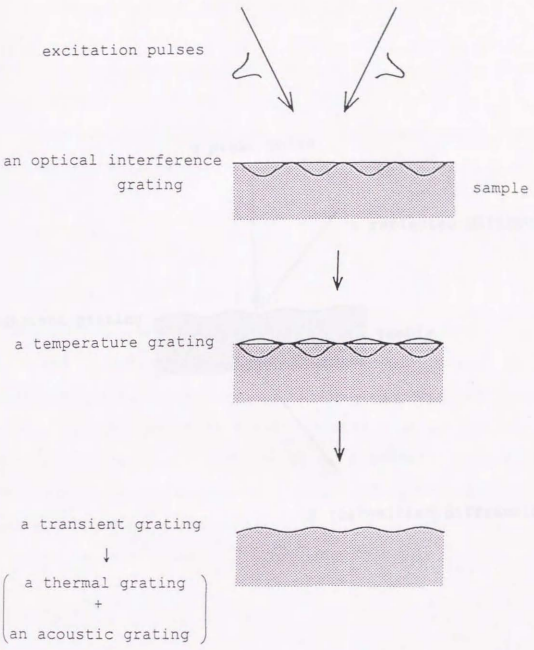

Fig. 2.1(a). Excitation of TG by interference of two pulse laser beams.

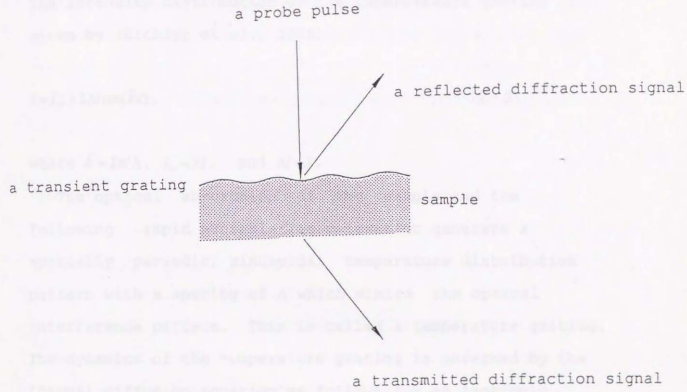

Fig. 2.1(b). Detection of TG by diffracting a third laser beam in a reflected or transmitted geometry.

angle of the two excitation pulses 2θ by

$$\Lambda = \lambda/2\sin\theta. \qquad (2 \cdot 1)$$

The intensity distribution of the interference grating is given by (Eichler et al., 1986)

$$I = I_{av} + 2\Delta I \cos(\bar{k}x), \qquad (2 \cdot 2)$$

where $\bar{k} = 2\pi/\Lambda$, $I_{av} = 2I$, and $\Delta I = I$.

The optical absorption of the sample and the following rapid nonradiative relaxation generate a spatially periodic, sinusoidal temperature distribution pattern with a spacing of Λ which mimics the optical interference pattern. This is called a temperature grating. The dynamics of the temperature grating is governed by the thermal diffusion equation as follows for an isotropic material (Nowacki, 1986),

$$k\nabla^2 T - C_s \rho \frac{\partial T}{\partial t} = -Q, \qquad (2 \cdot 3)$$

where T is the temperature, ρ is the equilibrium density, κ is the thermal conductivity, C_s is the heat capacity per unit mass at constant strain, and Q is the absorbed heat per unit time per unit volume induced from the excitation pulses.

The temperature grating induces elastic strain due to

the thermal expansion of the sample, which generates counterpropagating coherent acoustic waves (such as SAWs or interface waves) with a wavelength Λ and a nonpropagating thermal pattern. These are called an acoustic grating and a thermal grating, respectively. The dynamics of the acoustic and thermal gratings are governed by the thermoelastic equation, which can be written as follows for an isotropic, elastic, and homogeneous material (Nowacki, 1986),

$$\nabla^2\phi - \frac{\rho}{c_{11}}\frac{\partial^2\phi}{\partial t^2} = \frac{\gamma}{c_{11}}T, \qquad (2\cdot4)$$

$$\nabla^2\psi - \frac{\rho}{c_{44}}\frac{\partial^2\psi}{\partial t^2} = 0, \qquad (2\cdot5)$$

with

$$\mathbf{u} = \nabla\phi + \nabla\times\psi, \quad \nabla\cdot\psi = 0, \qquad (2\cdot6)$$

where ϕ and ψ are longitudinal and transverse potentials of the displacement vector $\mathbf{u}$, and they are related by eq. (2·6). T is the temperature distribution derived by eq. (2·3), ρ is the equilibrium density, c_{11} and c_{44} are the elastic constants and γ is a constant related to the elastic constants and the coefficient of linear volume expansion α_T by $\gamma = (3c_{11}-4c_{44})\alpha_T$. The solutions of eqs. (2·3)- (2·5) are discussed in detail in Chapter 5.

Thus a transient grating (TG) consisting of a thermal grating and an acoustic grating is formed.

2.1.2 Detection of the TGs

The TG can be probed by diffracting a third laser beam (probe pulse) in a transmitted or a reflected geometry as shown in Fig. 2.1 (b) for a transparent sample. But only the latter is suitable for an opaque sample. Then the TG can be seen as a transient transmission grating (TTG) or a transient reflecting grating (TRG), respectively. The TTG diffraction signal measures primarily the mean bulk properties of a sample since the probe beam passes through it. In contrast, the TRG diffraction signal is sensitive and selective to the properties of the sample surface or interface because it is dominated by diffraction from a thin region near the surface or interface which is some fraction of the optical wavelength (Fishman et al., 1993). As the first objective of this thesis is to study the properties of surfaces and interfaces as mentioned in Chapter 1, the TRG method is the primary concern in the following.

The light intensity of the first order diffraction of a TRG is detected as the TRG signal, which in general is time dependent. The time-dependent TRG signal (i. e. the TRG response) can be used to monitor the grating dynamics, such as the acoustic oscillations and their decay, the thermal diffusion, and other relaxation

dynamics. For an isotropic bulk sample, the TRG response can be approximately expressed by the following empirical equation (Harata et al., 1993b),

$$I_{TRG}(t) = R[I_e A g(t)]^2, \qquad (2 \cdot 7)$$

where I_e is the pump laser intensity, A is a constant depending on optical absorption, heat capacity, thermal conductivity, etc., R is optical reflectivity of the sample and

$$g(t) = \exp(-t/\tau_t) - r\cos[2\pi F(t + t_D)]\exp(-t/\tau_A). \qquad (2 \cdot 8)$$

In eq. (2・8), F is SAW frequency, t_D is onset time of the SAW generation, τ_t and τ_A are attenuation time constants for temperature and SAW, respectively, and r is the ratio of the acoustic effect to the thermal effect of their contribution to the grating amplitude. t_D is a parameter for a semiconductor sample, which is connected with the time of heat generating by the relaxation processes of photoexcited carriers. These parameters can be determined by fitting experimental curves of TRG responses to eq. (2・8) by a nonlinear least square method (Harata et al., 1993b). For an anisotropic sample or a film/substrate system, the corresponding parameters can be used as effective for the whole sample system. In this way, the acoustic and thermal properties of the sample system can be

extracted from the analyses of the experimental TRG responses.

2.2 Experimental arrangement

The TRG experimental arrangement is schematically illustrated in Fig. 2.2. A mode-locked Q-switched Nd:YAG laser (Quantronix, model 416) is used as the light source. The laser output is a train of mode-locked pulses. A single pulse (wavelength, 1064 nm; pulse width, 100 ps; intensity, ~20 μJ/pulse) from the train is selected and its frequency is doubled to produce a polarized visible light pulse (wavelength, 532 nm; pulse width, 84 ps and temporally nearly a Gaussian shape; repetition rate, 1.03KHz; intensity, ~5 μJ/pulse) (Harata, 1990).

The laser pulse is attenuated to less than 0.3 μJ per pulse to prevent the sample from being damaged. It is split into two beams by a partially reflective mirror. One of them is halved into two beams by a half mirror and they are used as two excitation pulses. The other one is used as a probe pulse. The two excitation pulses cross at the sample surface to form an optical interference pattern in a 60-μm-diameter spot.

The probe pulse is temporally delayed relative to the excitation pulses by a computer-controlled optical delay line (DL2). The largest delay time is 12.8 ns. The probe pulse is focused and incident normal to the surface on the interference pattern. The intensity is less than 10

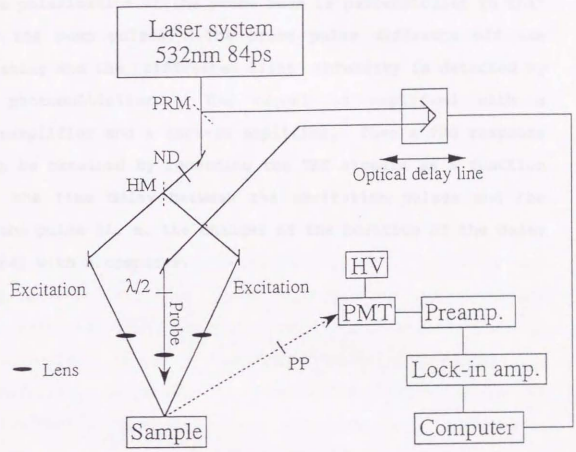

Fig. 2.2. Experimental arrangement of the laser-induced transient reflecting gratings. (HM) half mirror, (HV) high voltage, (HD) neutral density filter, (PRM) partial reflective mirror, (PMT) photomultiplier, (PP) photopolarizer, and (λ/2) half-wave plate.

nJ/pulse and the diameter of the spot size is about 40 μm. The polarization of the probe pulse can be rotated by a half-wave plate. In the experiments of the present thesis, the polarization of the probe beam is perpendicular to that of the pump pulses. The probe pulse diffracts off the grating and the diffracted light intensity is detected by a photomultiplier. The signal is amplified with a preamplifier and a lock-in amplifier. Then a TRG response can be obtained by recording the TRG signals as a function of the time delay between the excitation pulses and the probe pulse (i. e. the changes of the position of the delay line) with a computer.

Chapter 3

Analyses of thermal and acoustic properties of ultrathin (thickness: 40 nm) nonimplanted and ion-implanted diamondlike carbon (DLC) films on multilayered substrates by the TRG technique

The transient reflecting grating (TRG) technique was applied to evaluate both nitrogen-ion-implanted and nonimplanted thin-film coatings (thickness: 40nm) of diamondlike carbon (DLC) on metallic multilayered substrates. Different TRG responses corresponding to the different nitrogen ion doses were observed. Hypersonic surface wave velocities as well as the thermal diffusivities were obtained with a variety of grating spacings. Effective elastic moduli (Young's moduli) for the DLC coatings were given by using a theoretical treatment with a model. Nitrogen ion implantation hardened the DLC coating (Shen et al., 1994; Shen et al.,1995a).

3.1 Introduction

In recent years, diamondlike carbon (DLC) films have received considerable attention, being the subject of extensive investigations owing to their unique properties, which promise diverse applications. Their properties include extreme microhardness, resistance to corrosive chemicals, low electric conductivity, high wear resistance, low friction coefficient, high thermal conductivity, and excellent optical properties (Robertson, 1992; Wu, 1992; Nakaue et al., 1992; Savvides and Bell, 1992; Blech and Wood, 1993; Lettington, 1993). Attempts have been made to use DLC films of a few tens of nanometers in thickness as protective overcoats for magnetic disk media and wear coatings on magnetic recording heads (Lettington, 1993; Yamamoto, 1993; Marchon et al., 1991). With applications come a desire to evaluate the practical properties, such as optical, thermal, and elastic properties (such as Young's moduli), of ultrathin DLC films; however, as mentioned in Chapter 1, to the author's knowledge, it is really difficult to noninvasively measure the physical parameters of such thin films on a substrate by traditional methods, especially when the substrate has a multilayered structure, such as a magnetic disk.

As mentioned in Chapter 1, the TRG technique has been successfully utilized to investigate thermal and elastic properties of either bulk or thin films as a non-contact and non-destructive method by several researchers (Harata et al., 1990; Käding et al., 1993; Duggal et al., 1992a and 1992b). However, to the author's knowledge, in these reports only thin films with thicknesses on the order of 1

μm were studied by the TRG technique. In this chapter, the capabilities and potentials of the TRG technique were explored and demonstrated in studying the characteristics of ultrathin films with thicknesses of a few dozen nm. Diamondlike carbon thin-film coatings (thickness: 40nm) deposited on multilayered substrates were used as samples. Three kinds of samples with different nitrogen-ion-implanted doses and a nonimplanted sample were measured and different TRG responses were observed. Using a variety of grating spacings, hypersonic surface wave velocities and thermal diffusivities were extracted experimentally. By developing a model, effective elastic moduli for the DLC coatings were obtained. It was observed that for a high nitrogen-ion-implanted dose, the DLC coating was hardened relative to the nonimplanted sample. The work showed that the characteristic properties of DLC thin-film coatings with various ion doses can be evaluated by this TRG technique.

3.2 Results and Analyses

3.2.1 Samples

The samples measured were DLC coatings (thickness: 40nm) deposited by a chemical vapor deposition technique on metallic multilayered substrates (Co/Cr/plating of Ni and P alloy). Layer thicknesses were about 30nm for Co, 150nm for Cr and 10μm for Ni-P alloy and they were deposited on an aluminum plate of 1mm thickness. Such multilayered

systems are commonly used for commercial magnetic disks. Ion beams with 10keV energy and 68mA/cm^2 current were used for nitrogen implantation to the DLC coatings with doses of 2×10^{17}, 5×10^{17}, and 2×10^{18} atoms/cm^2. It has been reported that at an implantation energy of 10keV, when the dose is smaller than 10^{16} atoms/cm^2, nitrogen ions are distributed in the DLC coatings at depths of about 15nm±5nm under the surface (Doyama and Yamamoto, 1987; Dearnaley et al., 1973). For the ion doses used in the present research, however, nitrogen ions were closer to the surface than this because of sputtering (Doyama and Yamamoto, 1987). In the present experiment, the optical skin depth of the excitation pulse in the nonimplanted sample was about 50nm with the optical absorption coefficients of 4×10^4/cm for DLC film (Lettington, 1993) and 8.7×10^5/cm for Co layer (Gray, 1972). For the implanted samples, the corresponding optical skin depth became smaller than 50nm since the optical absorption coefficients of the implanted DLC films became larger.

3.2.2 Evaluation of the thermal properties of DLC films

For a nonimplanted sample, typical TRG responses with grating spacings of 0.86, 1.3, 2.27 and 3.96 μm are shown in Fig. 3.1. A single mode of the surface acoustic wave (SAW), i. e. the Rayleigh-like mode (Farnell and Alder, 1972; Shen et al., 1993), was excited on each sample. The SAW velocities were extracted by fitting the experimental TRG curves to an empirical equation (i. e. eq. (2.8)) with

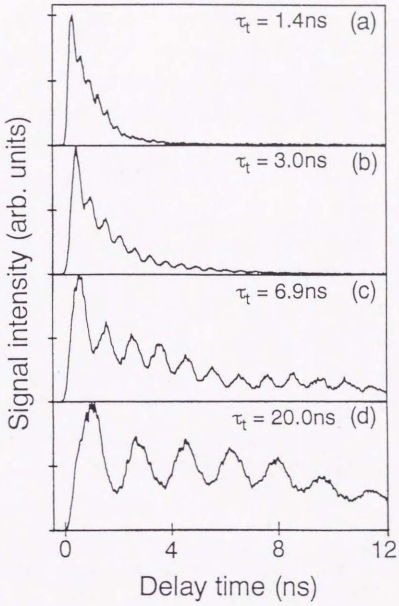

Fig. 3.1. Typical TRG responses of a nonimplanted DLC thin-film coating deposited on Co/Cr/plating of Ni and P multilayered substrates with (a) 0.86, (b) 1.3, (c) 2.27 and (d) 3.96 μm grating spacings. The corresponding attenuation time constants τ_t are 1.4, 3.0, 6.9, and 20.0 ns, respectively.

a nonlinear least square method as mentioned in the previous chapter. At the same time, the attenuation time constant τ_t of the thermal pattern, was also extracted as that of a slowly decaying component with an exponential function in the response (Harata et al., 1993b). As shown in Fig. 3.1, as the grating spacing became smaller, the TRG curves decayed faster (τ_t: 1.4, 3.0, 6.9 and 20.0ns). This resulted from heat flow in the grating direction, which, by equalizing the peak-to-null difference in temperature at the sample surface, is the dominant process causing the TRG signal decay. Thus, decay became faster with a smaller grating spacing (Marshall et al., 1992). The attenuation time constant τ_t is determined by the lateral thermal diffusivity k_l along the direction of the grating vector and the grating period Λ, which can be given by

$$\tau_t = \Lambda^2/(4\pi^2 k_l), \qquad (3 \cdot 1)$$

for bulk materials (Harata et al., 1990). The thermal diffusivity for homogeneous material can be directly determined from this equation by using the different decay times of the TRG curves corresponding to different grating spacings; however, a complicated mathematical analysis of the heat diffusion of the multilayer system is needed to extract the thermal diffusivities of the DLC coatings on multilayered substrates. In order to avoid this, the

effective lateral thermal diffusivity k_{eff} of the DLC coating/substrate system was obtained from the above equation using Λ and the corresponding τ_c. The effective diffusivity means the averaged value over the coating and the substrate within a vertical thermal penetration depth $h_{th}=(4k_v\tau_c)^{1/2}$ (Käding et al., 1993), in which k_v is the vertical thermal diffusivity and τ_c is the measured attenuation time constant. Then h_{th} can be written as

$$h_{th}=(k_v/k_l)^{1/2}\Lambda/\pi, \qquad (3\cdot2)$$

and it is proportional to the grating spacing. This means depth profiling of the thermal property can be obtained by varying the grating spacing. When the grating spacing is so small that h_{th} becomes smaller than the thickness of the DLC coating h_1 or approximately equal to h_1, the effective diffusivity is mainly determined by the coating diffusivity even if $\Lambda>h_1$. In this situation, the effective diffusivity is unchanged as Λ is decreased.

The results of the measured effective diffusivity for the DLC coating/substrate system are shown in Fig. 3.2. The lateral thermal diffusivity for the DLC coating was approximately determined as 0.13 cm^2/s. It is the effective diffusivity with smaller Λ which is almost unchanged with decreasing grating spacing. This result is on the same order as the literature values (Kuo et al., 1991).

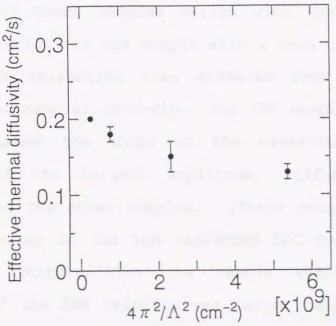

Fig. 3.2. Effective diffusivity for 40 nm DLC coating on Co/Cr/plating of Ni and P multilayered substrate versus the grating constant $4\pi^2/\Lambda^2$.

3.2.3 Characterization of ion-implanted DLC films

(a) Experimental results and discussions

Typical TRG responses for both the nitrogen ion implanted samples with different doses and the nonimplanted sample are shown in Figs. 3.3 and 3.4. The 1.3 and 0.86 μm grating spacings were used, respectively. The TRG responses of these samples varied with the implantation doses. Firstly, for the sample with a dose of $2\times10^{17}\,\mathrm{atoms/cm^2}$ the thermal relaxation time differed from that of the nonimplanted sample; secondly, for the sample with a dose of $5\times10^{17}\,\mathrm{atoms/cm^2}$ the shape of the waveform, i. e. the position of the largest amplitude, differed from the waveforms of the other samples. (There seemed to be some thermal barrier in the ion implanted DLC coating of this sample.) Thirdly, for the sample with a dose of $2\times10^{18}\,\mathrm{atoms/cm^2}$ the SAW velocity was larger than that of the other samples. These results can be qualitatively summarized as follows: as the bonding microstructure, the degree of lattice damage or disorder in the DLC films induced by the ion beams vary with the ion doses, the corresponding optical absorption coefficients, the thermal diffusivities and the acoustic muduli of the DLC films also change. These results remain to be investigated quantitatively. Later, changes of the SAW velocities and the elastic properties of the DLC coatings induced by nitrogen ion implantation are discussed.

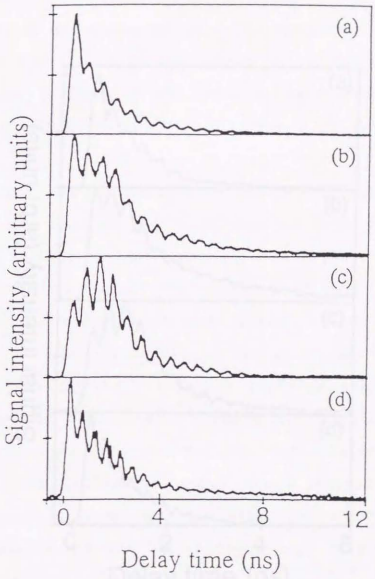

Fig. 3.3. Typical TRG responses of the nitrogen-ion-implanted DLC thin-film coatings deposited on Co/Cr/plating of Ni and P multilayered substrates with (b) 2×10^{17}, (c) 5×10^{17}, and (d) 2×10^{18} atoms/cm^2 implantation doses and (a) a nonimplanted sample. The grating spacing was 1.3 μm.

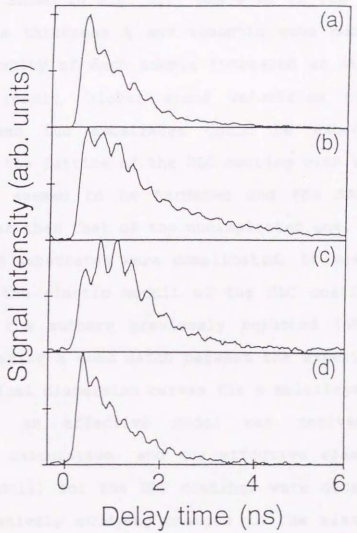

Fig. 3.4. Typical TRG responses of the nitrogen-ion-implanted DLC thin-film coatings deposited on Co/Cr/plating of Ni and P multilayered substrates with (b) 2×10^{17}, (c) 5×10^{17}, and (d) 2×10^{18} atoms/cm^2 implantation doses and (a) a nonimplanted sample. The grating spacing was 0.86 μm.

The SAW dispersion curves for both the nonimplanted DLC coating and the implanted one (dose, $2\times10^{18}\,\mathrm{atoms/cm^2}$) were obtained from measurements with a variety of grating spacings as shown in Fig. 3.5, where kh_1 is the product of the DLC film thickness h_1 and acoustic wave number $k=2\pi/\Lambda$. The SAW velocity of each sample increased as kh_1 increased. From this result, higher sound velocities of the DLC coatings than the substrates could be expected. In particular, the lattice of the DLC coating with the dose of $2\times10^{18}\,\mathrm{atoms/cm^2}$ seemed to be hardened and the SAW velocity became larger than that of the nonimplanted one. Since the multilayered substrates were complicated, it was difficult to extract the elastic moduli of the DLC coatings, using the method the authors previously reported (Shen et al., 1993), by making a good match between the experimental and the theoretical dispersion curves for a multilayered sample. Thus next, an effective model was derived for an approximate calculation, and the effective elastic moduli (Young's moduli) for the DLC coatings were determined for semiquantitatively studying changes in the elastic moduli by ion implantation.

(b) Theoretical analysis and discussion

In this TRG technique, SAWs were detected. The SAWs are modes of elastic energy propagating along the free surface, in which the displacement amplitudes of the acoustic waves decay in an exponential fashion with depth

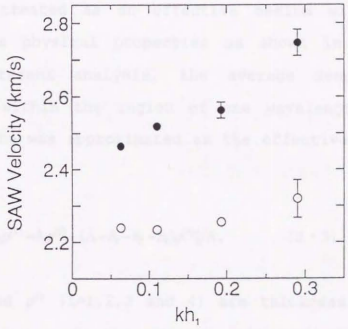

Fig. 3.5. SAW dispersion curves for a nonimplanted DLC coating (open circles) and an implanted sample with dose of 2×10^{18} atoms/cm^2 (dots), where kh_1 is the product of the DLC film thickness h_1 and acoustic wave number k ($=2\pi/\Lambda$).

beneath the surface. It follows that, essentially, almost all of the associated energy is concentrated within a distance of the order of a wavelength below the free surface (Farnell and Alder, 1972). In the present experiment, the samples were DLC coatings on metallic multilayered substrates as shown in Fig. 3.6(a). It was assumed that the characteristics of the SAW are determined only by the physical properties of the materials within the wavelength below the free surface. Then, the sample could be treated as an effective medium with effective homogeneous physical properties as shown in Fig. 3.6(b). In the present analysis, the average density of the materials within the region of one wavelength below the free surface was approximated as the effective density $\rho^{(\epsilon,\Lambda)}$, given by

$$\rho^{(\epsilon,\Lambda)} = [h_1\rho^{(1)} + h_2\rho^{(2)} + h_3\rho^{(3)} + (\Lambda - h_1 - h_2 - h_3)\rho^{(4)}]/\Lambda, \qquad (3 \cdot 3)$$

where h_i and $\rho^{(i)}$ (i=1,2,3 and 4) are thickness and density of each layer. In the present analysis, the literature values for densities of Co, Cr and Ni were used as $\rho^{(2)}$, $\rho^{(3)}$ and $\rho^{(4)}$ ($\rho^{(2)}$=8.8 g/cm^3, $\rho^{(3)}$=7.2 g/cm^3, and $\rho^{(4)}$=8.85 g/cm^3) (National Astronomical Observatory of Japan, 1990). $\rho^{(1)}$=1.9 g/cm^3 was adopted from the literature (Robertson, 1992) and commonly recognized density values for the DLC films. The corresponding effective longitudinal and shear elastic constants $c_{11}^{(\epsilon,\Lambda)}$, $c_{44}^{(\epsilon,\Lambda)}$ and the effective shear wave

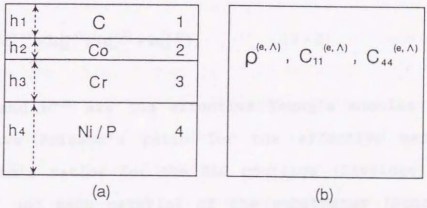

Fig. 3.6. An effective model for the DLC coating on a multilayered substrate (Co/Cr/plating of Ni and P alloy) at a SAW wavelength Λ: (a) The actual DLC coating system; (b) the effective model with the effective density $\rho^{(e,\Lambda)}$ and the effective elastic modulus $c_{11}^{(e,\Lambda)}$ and $c_{44}^{(e,\Lambda)}$.

velocity $V_t^{(e,\Lambda)}$ as well as the phase velocity of the Rayleigh-like mode $V_R^{(\Lambda)}$ can be written as follows (Farnell, 1969; Kolsky, 1963):

$$c_{11}^{(e,\Lambda)} = E^{(e,\Lambda)}(1-\sigma^{(e,\Lambda)})/[(1+\sigma^{(e,\Lambda)})(1-2\sigma^{(e,\Lambda)})], \qquad (3 \cdot 4)$$

$$c_{44}^{(e,\Lambda)} = E^{(e,\Lambda)}/2(1+\sigma^{(e,\Lambda)}), \qquad (3 \cdot 5)$$

$$c_{12}^{(e,\Lambda)} = c_{11}^{(e,\Lambda)} - 2c_{44}^{(e,\Lambda)}, \qquad (3 \cdot 6)$$

$$V_t^{(e,\Lambda)} = \sqrt{c_{44}^{(e,\Lambda)}/\rho^{(e,\Lambda)}}, \qquad (3 \cdot 7)$$

$$V_R^{(\Lambda)} = V_t^{(e,\Lambda)}(0.87c_{11}^{(e,\Lambda)} + 2c_{12}^{(e,\Lambda)})/(c_{11}^{(e,\Lambda)} + 2c_{12}^{(e,\Lambda)}), \qquad (3 \cdot 8)$$

where $E^{(e,\Lambda)}$ and $\sigma^{(e,\Lambda)}$ are the effective Young's modulus and the effective Poisson's ratio for the effective medium. Since Poisson's ratios for the DLC coatings (Savvides and Bell, 1993) and each material of the substrates (Schramm, 1962) are close to 0.3, the effective Poisson's ratio of 0.3 was used here. When the wavelength Λ becomes as small as the thickness of the DLC coating, the SAW is almost completely localized in the DLC coating, and these effective parameters become closer to the corresponding parameters of the DLC coatings. From eqs. (3・4) to (3・8), the measured SAW velocities $V_R^{(\Lambda)}$ for a variety of wavelengths were used to determine the corresponding effective Young's moduli of nonimplanted DLC coating and

nitrogen ion implanted (dose, 2×10^{18} atoms/cm^2) samples. These results are summarized in Table 3.1. The errors given for the Young's moduli are experimental errors for several (from 3 to 10) repetitive measurements. The effective Young's moduli of the nonimplanted DLC coating for the grating spacings from 0.86 μm to 3.96 μm were almost identical. On the other hand, the effective Young's moduli for the ion implanted sample were larger than those of the nonimplanted sample and they became larger as the wavelength decreased. This meant that the Young's moduli of the nonimplanted DLC film and the materials in the substrate were not greatly different from each other, while the modulus of the implanted DLC film (dose, 2×10^{18} atoms/cm^2) was much larger than those of the materials in the substrate. The DLC film with the implantation dose of 2×10^{18} atoms/cm^2 had become hardened, but the reason for this was not clear. Similar hardening has been reported for nitrogen ion implanted steel as dose was increased (Doyama and Yamamoto, 1987). The variation of the elastic properties with the increasing ion doses remains to be investigated quantitatively in connection with the corresponding lattice structures of the DLC coatings.

3.3 Conclusions

Diamondlike carbon (DLC) ultrathin coatings (40nm thick) on multilayered substrates, including nonimplanted and nitrogen ion implanted samples with various doses, have

Table 3.1. The effective Young's moduli of the nonimplanted and nitrogen ion implanted DLC coatings.

grating spacing (μm)		effective Young's modulus (GPa)
0.86		133±6
1.3	nonimplanted	129±1
3.96		131±1
0.86		187±2
1.3	implanted at a dose of	167±3
3.96	$2x10^{18}$ atoms/cm^2	160

been investigated by the transient reflecting grating (TRG) technique. The lateral thermal diffusivity of the DLC coating was determined. The SAW velocities with a variety of wavelengths were measured and corresponding effective Young's moduli were calculated by establishing an effective model. The nitrogen ion implantation at higher dose hardened the DLC coating. The TRG technique is applicable to non-destructive characterization of ultrathin coatings of probably less than 10nm in thickness. By analyzing the TRG responses with a variety of grating spacings, depth profiling of thermal and acoustic properties is also possible for a coating/substrate system, even if the substrate has a multilayered structure. This means that the TRG technique is suitable for characterization of surfaces and interfaces of multilayered systems and structurally gradient materials. The technique may provide new evaluation criteria in material processing for micro-electronics, optical computing, micro-machining and so on.

Chapter 4

Evaluation of the acoustic properties of the intermediate layer next to the surfaces layer for ultrathin multilayered films (Au/Cr/quartz) as well as determination of the thicknesses of thin metallic films (Au/soda lime glass) with the TRG technique

Gigahertz surface acoustic waves (the Rayleigh-like modes) have been optically generated and detected on ultrathin metallic single-layer and multilayered films attached to glass substrates using the laser-induced transient reflecting grating (TRG) technique. The dispersion relations of the excited Rayleigh-like modes could be constructed experimentally and theoretically. By finding the best fitting of the theoretical dispersion curves to the experimental data, this method can be used to deduce the elastic constants of ultrathin multilayered films, not only of the surface layer, but also of the intermediate layer (Shen et al., 1993).

4.1 Introduction

As mentioned in the previous chapters, the TRG technique has been extensively used to study various material properties in a wide variety of systems. In particular, it has been applied to characterize the acoustic and thermal properties of either bulk or film materials because of its advantages over more traditional ultrasonic methods, such as the lack of mechanical contact with samples and its excellent capability for generating high-power coherent ultrasonic waves of a few megahertz to 30GHz. Especially for samples with high optical densities such as opaque samples, the transient reflecting grating (TRG) technique has been very successful (Harata et al., 1990). In earlier work by Duggal et al. (1992) the TRG technique has been used to study the pseudo-Rayleigh modes of thin (0.92 μm to 5.81 μm) polyamide films attached to a silicon substrate. They established a theoretical method to extract the elastic properties of the films for single-layer film/substrate systems and demonstrated the feasibility of the TRG technique for determining the elastic constants of thin-film coatings.

For some technological purposes, it is of importance to be able to nondestructively measure the elastic properties of each layer, not only the surface layer, for a multilayered film system. This is a rather difficult and challenging problem. In the present chapter, it is established that the TRG technique can solve this problem.

The TRG technique was used to characterize Rayleigh-like modes (i.e., the pseudo-Rayleigh modes) of ultrathin single-layer or multilayered metal film/substrate systems, such as Ag/soda lime glass and Au/Cr/fused quartz, with film thicknesses of a few tens to a few hundreds of nanometers. By establish a theoretical model, the elastic properties of multilayered films (for example, the front Au and intermediate Cr films in an Au/Cr/fused quartz sample), besides those of a single-layer film, could be extracted by making a good match between the experimental and theoretical results for the acoustic dispersion relations. Furthermore, thicknesses of thin metallic films could be determined by this method.

4.2 Experimental results and discussion

The samples measured were Ag/soda lime glass (Ag film thickness: 27nm), and Au/Cr/fused quartz (Au surface layer, 300nm; Cr sublayer, 20nm), which are metallic multilayer materials. The films were prepared on isotropic substrates by a vapor deposition technique and they were also isotropic. Their typical surface TRG responses with 1.7 μm grating spacing are shown in Figs. 4.1 and 4.2. A fast-Fourier transform (FFT) method was used to provide frequency domain spectra of these TRG responses. As shown in Fig. 4.1, only a single acoustic wave mode was excited on the Ag/soda lime glass and there was one frequency corresponding to a phase

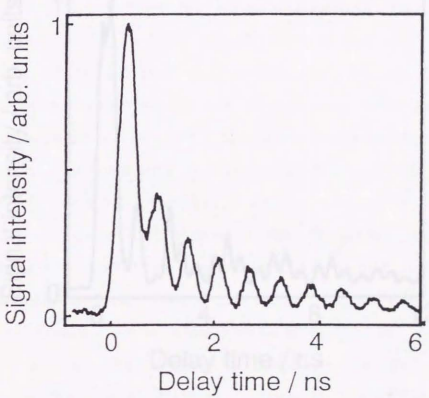

Fig. 4.1. Typical response of the TRG signal of a 27 nm Ag film on a soda lime glass substrate with 1.7 μm grating spacing.

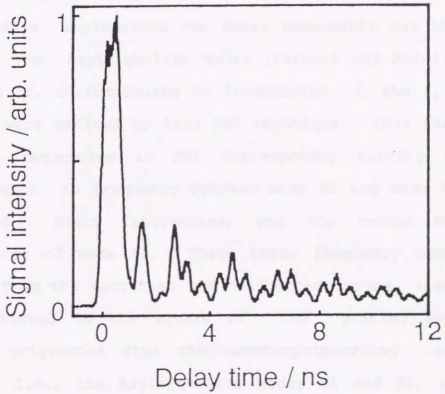

Fig. 4.2. Typical response of the TRG signal of an Au/Cr film on a fused quartz substrate with 1.7 μm grating spacing. The thicknesses of the Au surface layer and the Cr sublayer were 300 nm and 20 nm, respectively.

velocity of 2830 m/s in the FFT spectrum. This frequency was thought to correspond to the first Rayleigh-like mode (Farnell and Adler, 1972) of the Ag/soda lime glass sample and it was designated R1. On the other hand, in Fig. 4.2, more than one mode was excited on the surface of the Au/Cr/fused quartz sample. The FFT of this response revealed five frequencies as shown in Fig. 4.3. A reasonable explanation for these components was that the first two Rayleigh-like modes (Farnell and Adler, 1972), R1 and R2, corresponding to frequencies f_1 and f_2 in the FFT, were excited by this TRG technique. Thus the other three frequencies in FFT corresponded exactly to the difference in frequency between mode R1 and mode R2, the sum of their frequencies, and the second harmonic frequency of mode R1. These three frequency components arose from the fact that the diffracted probe signal was proportional to the square of the grating amplitude which originated from the counterpropagating acoustic waves, i.e., the Rayleigh-like modes R1 and R2, and the thermal spatial distribution. From a variety of fringe spacings (as shown in Fig. 4.4), the dispersion relations of the generated Rayleigh-like modes were experimentally determined. The results of modes R1 and R2 for the Au/Cr/fused quartz sample are plotted in Fig. 4.5 as circles.

4.3 Theoretical analyses and discussion

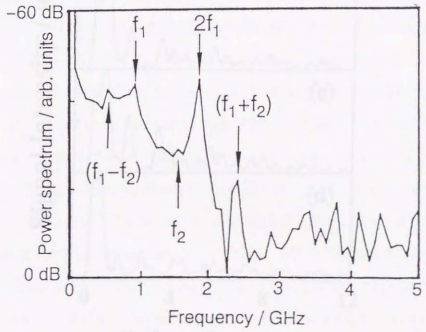

Fig. 4.3. Fourier transform of the TRG data of Fig. 4.2. Five frequency components corresponding to f_1, f_2, the difference between them, their sum, and the second harmonic of f1 are shown.

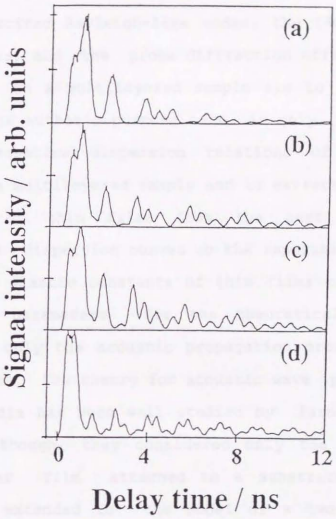

Fig. 4.4. Typical TRG responses of an Au/Cr film deposited on a fused quartz substrate with (a) 2.5, (b) 2.07, (c) 1.83 and (d) 1.34 μm grating spacings.

The TRG signal must be derived by treating the optical excitation and the probing processes, if the TRG response is to be analyzed theoretically and the dispersion relation of the excited Rayleigh-like modes, the TRG excitation efficiencies, and the probe diffraction efficiencies for each mode on a multilayered sample are to be understood. However, the author's purpose here is only to obtain the general theoretical dispersion relations of Rayleigh-like modes for a multilayered sample and to extract the elastic constants of thin films from the best fit of the theoretical dispersion curves to the experimental data, in which the elastic constants of thin films can be used as adjustable parameters for the theoretical calculation. Hence we only the acoustic propagation process is taken into account. The theory for acoustic wave propagation in layered media has been well studied by Farnell and Adler (1972); although, they considered only the model of a single-layer film attached to a substrate. Here the theory is extended to the model of a two-layered film deposited on a substrate. For simplicity isotropic theory is used because of the elastic isotropy of the films and substrates employed in the experiments.

A detailed theoretical calculation of the acoustic dispersion relations of Rayleigh-like modes on film/substrate systems in which there are two or fewer layers in the films was made (cf. Appendix 4.1). The calculated dispersion curves, v vs kh (where k is the

acoustic wave vector, h is the total thickness of films and v is the phase velocity), of the first five Rayleigh-like modes for the Au/Cr/fused quartz sample are shown in Fig. 4.5 as solid lines. With the values in the literature for the longitudinal and shear wave velocities of fused quartz (v_{Lq}=5.968 km/s and v_{Tq}=3.764 km/s) (National Astronomical Observatory of Japan, 1990), and for densities of fused quartz, Cr and Au (ρ_q =2.2 g/cm^3, ρ_{Au} = 19.32 g/cm^3, and ρ_{Cr} =7.193 g/cm^3) (National Astronomical Observatory of Japan, 1990), the longitudinal (v_L) and shear (v_T) wave velocities of Au film and Cr film were determined as v_{LAu}=3.44±0.01 km/s, v_{TAu}=1.233± 0.002 km/s, v_{LCr}=6.2±0.1 km/s, and v_{TCr}=3.8±0.1 km/s from the best fit of the theoretical dispersion curves of modes R1 and R2 to the experimental data. These values agreed well with the literature (National Astronomical Observatory of Japan, 1990), except for v_{LAu} which was about 6% larger than the reported value.

From Fig. 4.5, it was seen that the number of Rayleigh-like modes became larger as kh was increased, but when kh was very small, only the first mode R1 was present. This was the reason why only one Rayleigh-like mode R1 was excited for the Ag/soda lime glass sample, in which kh ≈ 0.07.

4.4 Determination of thicknesses of Au films on soda lime glasses

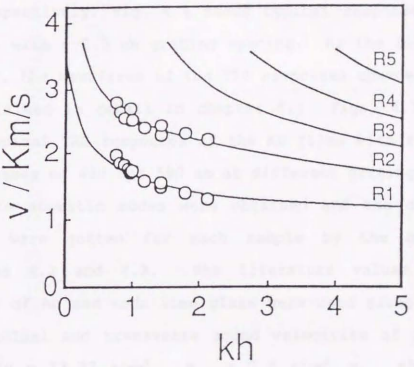

Fig. 4.5. Experimental data (circles) and theoretical Rayleigh-like mode dispersion curves (solid line) for an Au/Cr film on a fused quartz substrate with 300 nm Au film and 20 nm Cr film thicknesses. The elastic parameters of Au and Cr films used in generating the dispersion curves were optimized to obtain the best fit of the dispersion curves of R1 and R2 modes to the experimental data.

Using the same method mentioned above, determination of the thicknesses of Au film on soda lime glasses was also attempted. The thickesses of the films were determined by atomic absorption spectrometry as 25, 96, 430, 590, and 910 nm, respectively. Fig. 4.6 shows typical responses of the samples with a 2.5 μm grating spacing. As the film became thicker, the waveforms of the TRG responses changed. (This is explained in detail in chapter 5.) Figs. 4.7 and 4.8 show typical TRG responses of the Au films with respective thicknesses of 430 and 590 nm at different grating spacings. Only the acoustic modes were obtained and the dispersion curves were gotten for each sample by the method in sections 4.2 and 4.3. The literature values for the density of Au and soda lime glass were used along with the longitudinal and transverse sound velocities of soda lime glass (ρ_{Au}= 19.32 g/cm^3, ρ_{glass}= 2.5 g/cm^3, v_{Lglass}=5.639 km/s, v_{Tglass}=3.453 km/s) (National Astronomical Observatory of Japan, 1990), and the longitudinal and transverse sound velocities of Au film determined above for the Au/Cr/quartz sample (v_{LAu}=3.44 km/s, v_{TAu}=1.233 km/s). Only the thickness of the Au film was chosen as a free parameter and the theoretical dipersion curves were fitted to the experimental results. The thicknesses of the Au films could be determined from the best fit of the theoretical dispersion curves to the experimental data and the results are shown in Table 4.1. They were in reasonable agreement with those measured by the AAS method.

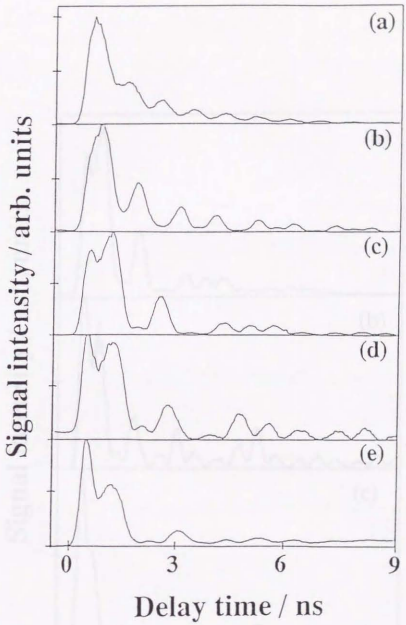

Fig. 4.6. Typical TRG responses of Au films with different thicknesses deposited on soda lime glass substrates. The grating spacing was 2.5 μm. The thicknesses of Au films measured by atomic absorption spectrometry (AAS) were (a) 25, (b) 96, (c) 430, (d) 590, and (e) 910 nm.

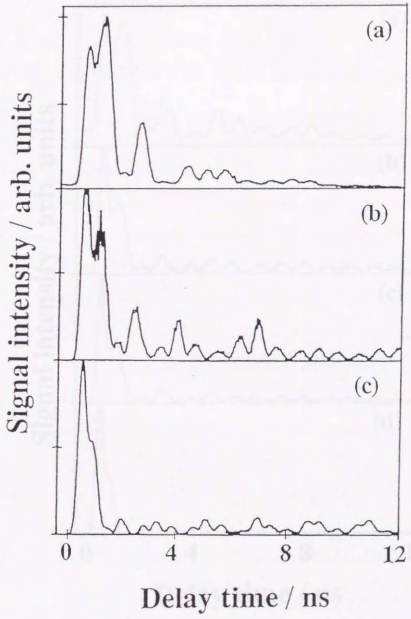

Fig. 4.7. Typical TRG responses of Au films (thickness: 430 nm) deposited on soda lime glass substrate with (a) 2.5, (b) 1.83, and (c) 1.34 μm grating spacings.

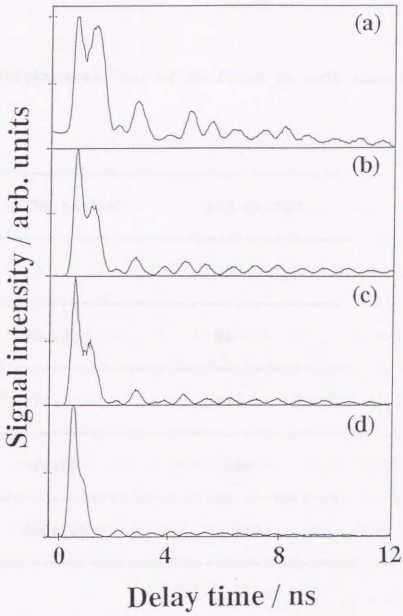

Fig. 4.8. Typical TRG responses of Au films (thickness: 590 nm) deposited on soda lime glass substrate with (a) 2.5, (b) 2.07, (c) 1.83, and (d) 1.34 μm grating spacings.

Table 4.1 Thicknesses (nm) of Au films on soda lime glasses.

sample	TRG method	AAS method
Au1	40	25
Au2	90±10	96
Au3	338	430
Au4	530±10	590
Au5	900±100	910

4.5 Conclusions

In this chapter, it was demonstrated that the TRG technique can be used to observe and study the coherent Rayleigh-like acoustic waves of GHz-order frequency on ultrathin multilayered metallic films. The dispersion relations of excited Rayleigh-like modes were constructed experimentally and theoretically. By finding the best fitting of the calculated dispersion curves for the modes excited in the TRG experiments to the experimentally determined velocity values, a method for deducing the elastic parameters (longitudinal and shear wave velocities) of each film in multilayer-film/substrate systems was described and applied to an Au/Cr/fused quartz sample. This method can also be used to determine thicknesses of thin films on substrates, such as the Au films on soda lime glass. The findings show that the TRG technique has a wide range of potential for applications in non-destructive characterization of metallic multilayered film samples, such as in the determination of elastic moduli and film thicknesses.

Appendix 4.1:

The coordinate system for a two-layer-film/substrate sample is shown in Fig. A.4.1. The direction of surface acoustic wave (SAW) propagation defined by $\mathbf{K}$, which was set by the interference pattern of the pump beams in the TRG experiment, is taken as the x_1 direction. The elastic wave equation for the particle displacement u_j along the axis x_j in the sample can be given as follows (Farnell and Adler, 1972):

$$\rho \frac{\partial^2 u_j}{\partial t^2} - c_{ijkl} \frac{\partial^2 u_k}{\partial x_i \partial x_l} = 0 \quad (i, j, k, l = 1, 2, 3), \qquad (A \cdot 4 \cdot 1)$$

where ρ is the density of the medium concerned and c_{ijkl} is the elastic stiffness tensor. The SAWs of interest here are those waves which decay with depth into the substrate and have constant phase and amplitude for each component along any line parallel to the x_2 axis. Thus the partial wave of the SAWs can be assumed as

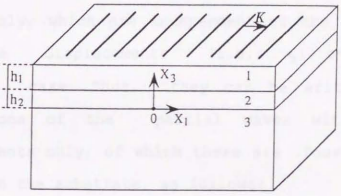

Fig. A.4.1. Coordinate system for SAW propagation in a two-layer-film/substrate sample. The thicknesses of the front and the intermediate films are h1 and h2, respectively. The acoustic wave vector **K** setup by the interference pattern of the pump beams in the TRG experiment is in the x_1 direction.

$$u_j = A_j \exp(ikbx_3)\exp[ik(x - vt)]. \qquad (A \cdot 4 \cdot 2)$$

By substituting eq.(A · 4 · 1) into eq.(A · 4 · 2), the solutions of three partial waves in the substrate and six in each layer are obtained. The Rayleigh-like modes are those solutions with "sagittal-plane" (Farnell and Adler, 1972) (i.e., x_1x_3 plane) displacements (i.e., u_1 and u_3) only, which are independent of the solutions with transverse displacements (i.e., u_2) only for the isotropic case. Thus, they can be written as linear combinations of the partial waves with ul and u3 displacements only, of which there are four in each layer and two in the substrate, as follows:

$$u_{1,3}^{(I)} = [D_n^{(I)} A_{1,3}^{(I,n)} \exp(ikb_n^{(I)} x_3)]\exp[ik(x_1 - vt)]$$

I=1,2,3

n=4, for I=1,2

n=2, for I=3, (A · 4 · 3)

where I is the layer number in the sample shown in Fig. A.4.1, and the summation index n in eq.(A · 4 · 1) has four

labels for the four partial waves in each layer, and two labels for the two partial waves in the substrate, and $D_n^{(I)}$ are the weighting factors of the partial wave n in layer I. The weighting factors can be determined under the boundary conditions that u_1, u_3 and the normal components of the stress are continuous at $x_3 = 0$ and $x_3 = h_2$, and that the normal components of the stress vanish for $x_3 = h_1 + h_2$. By imposing these boundary conditions, a set of ten homogeneous algebraic equations is obtained in the ten weighting factors $D_n^{(I)}$, which are expressed in matrix form as follows:

$$G \cdot H = 0, \qquad (A \cdot 4 \cdot 4)$$

where

$G=$

$$
\begin{pmatrix}
E_1^T R_1^+ & -R_2^+ & -E_1^T R_1^- & -R_2^- & -E_2^T R_3^+ & R_4^+ & E_2^T R_3^- & R_4^- & 0 & 0 \\
-R_1^+ & -E_1^L R_2^+ & -R_1^- & E_1^L R_2^- & R_3^+ & E_2^L R_4^+ & R_3^- & -E_2^L R_4^- & 0 & 0 \\
F_1 R_1^+ & 2E_1^L R_2^+ & F_1 R_1^- & -2E_1^L R_2^- & -R_7 F_2 R_3^+ & -2R_7 E_2^L R_4^+ & -R_7 F_2 R_3^- & 2R_7 E_2^L R_4^- & 0 & 0 \\
2E_1^T R_1^+ & -F_1 R_2^+ & -2E_1^T R_1^- & -F_1 R_2^- & -2R_7 E_2^T R_3^+ & R_7 F_2 R_4^+ & 2R_7 E_2^T R_3^- & R_7 F_2 R_4^- & 0 & 0 \\
0 & 0 & 0 & 0 & E_2^T & -1 & -E_2^T & -1 & E_3^T & 1 \\
0 & 0 & 0 & 0 & -1 & -E_2^L & -1 & E_2^L & 1 & -E_3^L \\
0 & 0 & 0 & 0 & F_2 & 2E_2^L & F_2 & -2E_2^L & -R_8 F_3 & 2R_8 E_3^L \\
0 & 0 & 0 & 0 & 2E_2^T & -F_2 & -2E_2^T & -F_2 & 2R_8 E_3^T & R_8 F_3 \\
F_1 R_5^+ & 2E_1^L R_6^+ & F_1 R_5^- & -2E_1^L R_6^- & 0 & 0 & 0 & 0 & 0 & 0 \\
2E_1^T R_5^+ & -F_1 R_6^+ & -2E_1^T R_5^- & -F_1 R_6^- & 0 & 0 & 0 & 0 & 0 & 0
\end{pmatrix}
$$

(A・4・5)

$$H = \begin{bmatrix} D_1^{(1)} \\ D_2^{(1)} \\ D_3^{(1)} \\ D_4^{(1)} \\ D_1^{(2)} \\ D_2^{(2)} \\ D_3^{(2)} \\ D_4^{(2)} \\ D_1^{(3)} \\ D_2^{(3)} \end{bmatrix} \qquad (A \cdot 4 \cdot 6)$$

$$E_j^T = i[1-(v/v_{tj})^2]^{1/2} \qquad j=1,2,3 \qquad (A \cdot 4 \cdot 7)$$

$$E_j^L = i[1-(v/v_{lj})^2]^{1/2} \qquad j=1,2,3 \qquad (A \cdot 4 \cdot 8)$$

$$F_j = 1-(E_j^T)^2 \qquad j=1,2,3 \qquad (A \cdot 4 \cdot 9)$$

$$R_1^{\pm} = \exp(\pm mE_1^T) \qquad j=1,2,3 \qquad (A \cdot 4 \cdot 10)$$

$$R_2^{\pm} = \exp(\pm mE_1^L) \qquad j=1,2,3 \qquad (A \cdot 4 \cdot 11)$$

$$R_3^{\pm} = \exp(\pm mE_2^T) \qquad j=1,2,3 \qquad (A \cdot 4 \cdot 12)$$

$$R_4^{\pm} = \exp(\pm mE_2^L) \qquad j=1,2,3 \qquad (A \cdot 4 \cdot 13)$$

$$R_5^{\pm} = \exp(\pm nE_1^T) \qquad j=1,2,3 \qquad (A \cdot 4 \cdot 14)$$

$$R_5^{\pm} = \exp(\pm nE_1^L) \qquad j=1,2,3 \qquad (A \cdot 4 \cdot 15)$$

$$R_7 = c_{44}(2)/c_{44}(1) \qquad j=1,2,3 \qquad (A \cdot 4 \cdot 16)$$

$$R_8 = c_{44}(3)/c_{44}(2) \qquad j=1,2,3 \qquad (A \cdot 4 \cdot 17)$$

$$m = ikh_2 \qquad (A \cdot 4 \cdot 18)$$

$$n = ikh \qquad (A \cdot 4 \cdot 19)$$

$$h = h_1 + h_2, \qquad (A \cdot 4 \cdot 20)$$

and $c_{44}(j)$, v_{ij}, and v_{ij} (j=1,2,3) are the shear modulus, the longitudinal wave velocity, and the shear wave velocity of layer j, respectively. h_1 and h_2 are the thicknesses of the front and the intermediate films, respectively, and v is the phase velocity of a Rayleigh-like mode.

Normal mode solutions of eq.(A・4・3) occur when

$$\det(G)=0. \qquad (A \cdot 4 \cdot 21)$$

Thus by solving eq.(A・4・21) numerically, the dispersion curves (v vs kh) can be obtained for the various Rayleigh-like modes of a two-layer-film/substrate system. The dispersion relation for a one-layer-film/substrate sample can be obtained easily by setting $h_2 = 0$ in eq.(A・4・21), which is the same as the result obtained by Farnell and Adler (1972).

Chapter 5

Analysis of interfaces (liquid/solid, gas/solid etc.) by the TRG technique: A general theory for extracting the TRG responses and potential of the TRG technique to analyze electrochemical interfaces

The transient reflecting grating (TRG) technique has been used to analyze metallic thin films on substrates or liquid/solid interfaces. A general theory was developed to calculate the TRG diffraction signals on interfaces (i. e., gas/solid, liquid/solid or solid/solid surfaces). With this theory, the TRG response for a sample of Au film/soda lime glass was calculated, and the results agreed very well with the experimental ones. For the first time, it was found theoretically and experimentally that along with surface acoustic waves, longitudinal acoustic pulses normal to the sample surfaces could be generated and detected at the surfaces of thin films by the TRG technique. By using the time intervals of two neighboring longitudinal acoustic pulses, thicknesses or longitudinal acoustic waves for opaque thin films could be determined by this method. The TRG technique shows a potential use for detecting thermal diffusivities, acoustic

wave (transverse and longitudinal) velocities and thicknesses at the same time for opaque thin films. Furthermore, it is proposed that this method can be applied to analyze electrochemical interfaces *in situ*, such as changes in the properties of electric double layers versus electrode potentials (Shen et al., 1995b).

5.1 Introduction

The transient grating (TG) technique has proven to be a powerful tool for studying a wide variety of material properties over the past decade (Eichler et al., 1986; Fayer, 1986). As it was mentioned earlier, the TG technique can be divided into two kinds: the transient transmission grating technique (TTG) and the transient reflecting grating technique (TRG). The TRG technique is very sensitive and selective to charaterization of surface or interface properties. The TRG technique was successfully applied to the study of elastic and thermal properties for ultrathin near-surface layers of less than 100nm thicknesses as mentioned in Chapters 3 and 4 (Shen et al., 1993; Shen et al., 1994; Shen et al., 1995a). Harata et al. (1995) have used this method to study electrochemical interfaces and they have observed some interesting phenomena such as that the measured TRG

waveforms for the gold/0.1M $HClO_4$ aqueous solution interface changed with different electrode potentials. These results show the feasibility of the TRG technique for applications to characterization of electrochemical interfaces. However, some theoretical analyses are needed to explain these experimental results further.

Some researchers (Kasinski et al, 1988; Faran et al., 1990; Duggal et al., 1992b), have made theoretical analyses about the SAWs or liquid/solid interface waves induced by the TG technique. However, in their analyses, the time scales for thermal diffusion were assumed to be much longer than the experimental time scales or than those of acoustic oscillations and damping, and the spatially modulated temperature fields induced by the TG method were approximated as unit step functions of time. These assumptions are not applicable to those materials with larger thermal diffusivities, such as metals. In addition, none of these studies gave a strict solution of the elastic displacement at the sample surface or interface induced by the TGs.

In this chapter, by using Laplace transforms in time, a method is presented to derive strict analytical expressions, which are functions of complex frequency s and position, of temperature fields and transverse and longitudinal potentials of elastic displacement vectors

induced by the TRG technique for a liquid/film/ substrate system or a gas/film/ substrate system. Then by means of a numerical inverse Laplace transform method, numerical solutions of temperature field or displacements can be obtained as functions of time at any position, especially at the interfaces (gas/solid, liquid/solid and solid/solid etc.). As an example, by supposing the TRG signals are proportional to the square of the normal elastic displacements at the sample surfaces, the TRG signal was calculated at the surface of an Au thin film (thickness, 430nm) attached to a soda lime glass substrate. The theoretical result agreed very well with the experimental result of the TRG signal. Theoretically and experimentally, it was found that along with SAWs, longitudinal acoustic pulses normal to the film surface could be excited and detected in film/substrate systems by the TRG technique. To the author's knowledge, this is the first demonstration of generation and detection of longitudinal acoustic pulses normal to the sample surface by the TRG method. This means that thicknesses or longitudinal wave velocities of ultrathin opaque films can be determined by detection of these acoustic pulses. Furthermore, the TRG technique can be applied to analyze electrochemical interfaces *in situ*, such as changes in the properties of electrode/solution interfaces with the electrode potentials.

5.2 Theory

The system of a solid film attached to a substrate and in contact above with a liquid was considered here (Fig. 5.1). Layer numbers 1, 2 and 3 refer to liquid, film and substrate. The solid substrate and liquid were assumed to extend far enough so that their outer boundaries could be considered to be infinite. The liquid and the film were assumed to be transparent and opaque, respectively. The two excitation laser pulses were incident in the liquid/film interface and they were absorbed by the film. The laser spot size was assumed to be much larger than the interference grating spacing and its edge effects were neglected, which was reasonable for the present experimental conditions. The direction of the optical interference grating vector **k** was taken as x and the direction normal to the interface was taken as z.

Assuming that the film and the substrate were isotropic and linearly elastic, and the liquid was isotropic and inviscid, the thermoelastic equations for this system could be written as follows:

$$k_{th}\nabla^2 T - C_A \rho \frac{\partial T}{\partial t} = -Q, \qquad (2 \cdot 3)$$

$$\nabla^2 \phi - \frac{\rho}{c_{11}} \frac{\partial^2 \phi}{\partial t^2} = \frac{\gamma}{c_{11}} T, \qquad (2 \cdot 4)$$

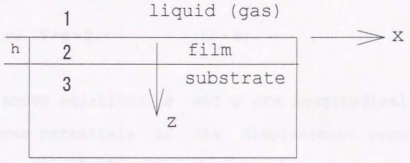

Fig. 5.1 Coordination system for a liquid/film/ substrate sample. The thickness of the film was h. The transient grating vector induced by the interference of two excitation beams was in the x direction.

$$\nabla^2\psi - \frac{\rho}{c_{44}}\frac{\partial^2\psi}{\partial t^2} = 0, \qquad (2 \cdot 5)$$

with

$$\mathbf{u} = \nabla\phi + \nabla\times\psi, \quad \nabla\cdot\psi = 0. \qquad (2 \cdot 6)$$

In the above equations, ϕ and ψ are longitudinal and transverse potentials of the displacement vector $\mathbf{u}$ as shown in eq. (2 · 6). For the liquid layer 1, the transverse potential ψ does not exist. T is the temperature change relative to room temperature, ρ is the equilibrium density, k_{th} is the thermal conductivity, C_ε is the heat capacity per unit mass at constant strain, and Q is the absorbed heat per unit time per unit volume induced from the excitation pulses. c_{11} and c_{44} are the elastic constants and γ is a constant related to the elastic constants and the coefficient of linear volume expansion α_T by $\gamma = (3c_{11} - 4c_{44})\alpha_T$.

For the coordinate system shown in Fig. 5.1, the solutions will be independent of y. Thus there is only a nonzero component along the y direction for ψ in layers 1 and 2, designated as ψ_y. Then the Eqs. (2 · 3)-(2 · 5) can be rewritten as follows:

$$D_x^{(i)}\frac{\partial^2 T^{(i)}}{\partial x^2}+D_z^{(i)}\frac{\partial^2 T^{(i)}}{\partial z^2}-\frac{\partial T^{(i)}}{\partial t}=\begin{cases}0, & \text{for i=1, 3}\\ -Ae^{-\beta z}(1+\cos\bar{k}x)\delta(t), & \text{for i=2}\end{cases} \qquad (5\cdot 1)$$

$$\nabla^2\phi^{(i)}-\frac{1}{(v_l^{(i)})^2}\frac{\partial^2\phi^{(i)}}{\partial t^2}=\frac{\gamma^{(i)}}{c_{11}^{(i)}}T^{(i)}, \quad \text{for i=1,2 and 3} \qquad (5\cdot 2)$$

$$\nabla^2\psi_y^{(i)}-\frac{1}{(v_t^{(i)})^2}\frac{\partial^2\psi_y^{(i)}}{\partial t^2}=0, \quad \text{for i=2,3} \qquad (5\cdot 3)$$

where $A=(1/\rho^{(2)}C_s^{(2)})Q$, $v_l^{(i)}$ and $v_t^{(i)}$ are the longitudinal and transverse wave velocities of the corresponding layer, and $D_x^{(i)}$ and $D_z^{(i)}$ are the thermal diffusivities along x and z directions for the layer i.

Since the spatial distribution profiles of the temperature and dispalcements in the sample along the x direction are the same as the optical interference grating, the temperature $T^{(i)}(x,z,t)$ and the potentials $\phi^{(i)}(x,z,t)$ and $\psi_y^{(i)}(x,z,t)$ can be reasonably assumed as the following expressions.

$$T^{(i)}=T_1^{(i)}(z,t)\cos(\bar{k}x)+T_0^{(i)}(z,t), \quad (i=1,\ 2,\ 3) \qquad (5\cdot 4)$$

$$\phi^{(i)}=\phi_1^{(i)}(z,t)\cos(\bar{k}x)+\phi_0^{(i)}(z,t), \quad (i=1,\ 2,\ 3) \qquad (5\cdot 5)$$

$$\psi_y^{(i)}=\psi_{y1}^{(i)}(z,t)\sin(\bar{k}x)+\psi_{y0}^{(i)}(z,t), \quad (i=2,\ 3) \qquad (5\cdot 6)$$

where the components with subscript 1 contribute to the TGs (i. e., the thermal and acoustic gratings), while those with 0 make no contribution. Therefore, the periodic, spatially modulated components with subscript 1 are the only concern. In the following, eq. (5・4) is solved to obtain $T_1^{(1)}(z,t)$ first, and eqs. (5・5) and (5・6) are solved to get the acoustic displacements at the interfaces second. Then the TRG signals are calculated for some samples. Finally the results are discussed and applications of the TRG technique are presented.

5.2.1 Transient temperature field generated by the TGs

Laplace transforms for the time variables were used from eq. (5・1) to eq. (5・6). By substituting eq. (5・4) into (5・1) and using the boundary conditions that the temperatures and heat fluxes are continuous at the liquid/film and film/substrate interfaces, analytical expressions for $T_1^{(1)}(z,s)$ were derived strictly (c.g. Appendix 5.1). The above results can be applied to a gas/film/ substrate system easily by using the corresponding physical parameters of the gas instead of the liquid in layer 1. Numerical solutions for transient temperature $T_1^{(1)}(z,t)$, which correspond to the thermal grating, could be obtained using a numerical method of inverse Laplace transforms (Hosono, 1984).

As an example, the transient temperatures T_1 at the interfaces for water/Au film/soda lime glass systems were calculated with the values in the literature (National Astronomical Observatory of Japan, 1990) for densities $\rho^{(1)} = 1.0\ g/cm^3$, $\rho^{(2)} = 19.3\ g/cm^3$, and $\rho^{(3)} = 2.5\ g/cm^3$, thermal diffusivities $D_x^{(1)} = D_z^{(1)} = 1.447 \times 10^{-3}\ cm^2/s$, $D_x^{(2)} = D_z^{(2)} = 1.302\ cm^2/s$, $D_x^{(3)} = D_z^{(3)} = 9.6 \times 10^{-3}\ cm^2/s$, thermal conductivities $k_{th}^{(1)} = 0.56 \times 10^{-2}\ W \cdot cm^{-1} \cdot K^{-1}$, $k_{th}^{(2)} = 3.15\ W \cdot cm^{-1} \cdot K^{-1}$, $k_{th}^{(3)} = 1.4 \times 10^{-2}\ W \cdot cm^{-1} \cdot K^{-1}$, and the optical absorption density $\beta = 4.55 \times 10^5\ cm^{-1}$ for Au with different Au film thicknesses (30, 100, and 300nm) at a grating spacing of 2.0μm, as shown in Fig. 5.2. After the excitation pulses were incident on the samples, the temperatures T_1 of the water/Au film interfaces decreased sharply while those of the film/ substrate interfaces increased rapidly within a short time. They were mainly induced by thermal diffusions in the Au films along the z direction and they resulted in uniform temperature distributions in the depth of the Au films. Then the temperatures T_1 decreased slowly due to the thermal diffusions along the thermal gratings in the x direction. This became slower as the grating spacings were made larger as shown in Fig. 5.3. From these results, it was known that the thermal gratings in metallic films, such as Au films, decay fast and exist almost only within the first 1 ns. Similar results were obtained for air/Au film/soda lime glass systems. Since thermal diffusions in both water and air are much slower than those in Au films,

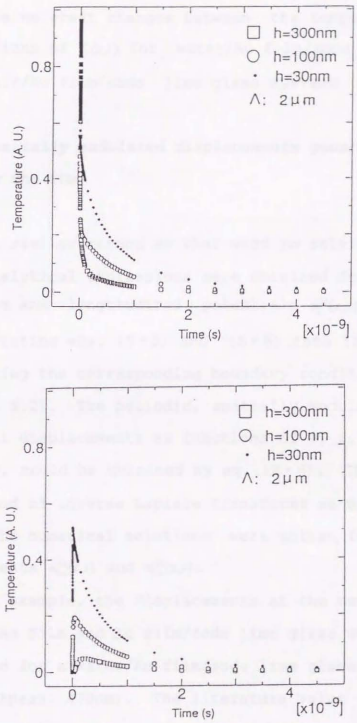

Fig. 5.2. The time responses of the amplitudes of spatially modulated temperature T_1 induced by the transient grating at (a) the water/Au film interfaces, (b) the Au film/soda lime glass interfaces for water/Au film/soda lime glass systems. The grating spacing was 2 μm.

there were no great changes between the temperature distributions of $T_1(z,t)$ for water/Au film/soda lime glass and for air/Au film/soda lime glass systems.

5.2.2 Spatially modulated displacements generated by the TGs

With a similar method as that used in solving eq. (5・1) above, analytical expressions were obtained for the transverse and longitudinal potentials $\phi_1^{(i)}(z,s)$ and $\psi_{y1}^{(i)}(z,s)$ by substituting eqs. (5・5) and (5・6) into (5・2) and (5・3) and using the corresponding boundary conditions (Appendix 5.2). The periodic, spatially modulated parallel and normal displacements as functions of s, i. e. $u_{1x}^{(i)}(z,s)$ and $u_{1z}^{(i)}(z,s)$, could be obtained by eq. (2・6). Then using the same method of inverse Laplace transforms as mentioned above, the numerical solutions were gotten for the displacements $u_{1x}^{(i)}(z,t)$ and $u_{1z}^{(i)}(z,t)$.

As an example, the displacements at the two interfaces of water/Au film and Au film/soda lime glass were calculated for a water/Au film/soda lime glass system (Au film thickness: 430nm). The literature value (National Astronomical Observatory of Japan, 1990) for longitudinal and transverse velocities $v_l^{(1)}=1500$ m/s, $v_l^{(2)}=3240$ m/s, $v_l^{(3)}=5100$ m/s, $v_t^{(2)}=1220$ m/s, $v_t^{(3)}=2840$ m/s, and the coefficients of linear volume expansion $\alpha_T^{(1)}=0.21\times10^{-3}$, $\alpha_T^{(2)}=4.26\times10^{-5}$, $\alpha_T^{(3)}=2.7\times10^{-5}$ were used for the calculation. The results are

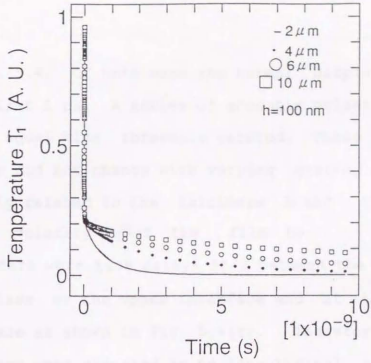

(a)

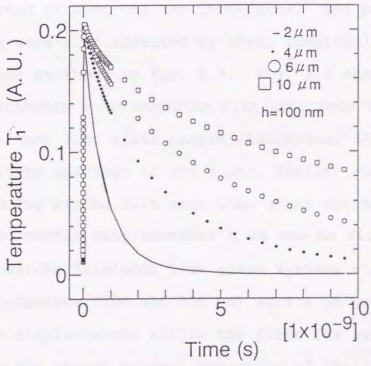

(b)

Fig. 5.3. The time responses of the amplitudes of spatially modulated temperature T_1 induced by the transient grating method at (a) the water/Au film interfaces, (b) the Au film/soda lime glass interfaces for a water/Au film/soda lime glass system. The Au film thickness was 100 nm. The grating spacings were 2, 4, 6 μm.

shown in Fig. 5.4. Of note were the normal displacements within the first 1 ns. A series of acoustic pulses separated by equal time intervals existed. These time intervals Δt did not change with varying grating spacings and were only related to the thickness h and the longitudinal velocity $v_l^{(2)}$of the film by $\Delta t=2h/v_l^{(2)}$. There were time delays $\Delta t/2$ between the acoustic pulses at the upper interface and at the lower interface as shown in Fig. 5.4(c). Therefore these acoustic pulses were expected to be longitudinal acoustic echoes reflected between the two interfaces. The parallel displacements were also affected by these longitudinal acoustic pulses as shown in Fig. 5.5. Fig. 5.6 shows the normal displacements u_z at water/Au film interface for a water/Au film/soda lime glass sample (thickness: 500nm) at different grating spacings (2 and 4 μm). Similar results were obtained for air/Au film/soda lime glass systems. Fig. 5.7 shows the normal displacements u_z at the Au film surfaces for air/Au film/soda lime glass systems with different thicknesses (200 and 500 nm) at a 4 μm grating spacing. The displacements within the first 1ns were mainly due to the steady thermal expansion of the thermal grating and the longitudinal acoustic echoes, while the displacements after 1 ns resulted from interface acoustic waves or SAWs.

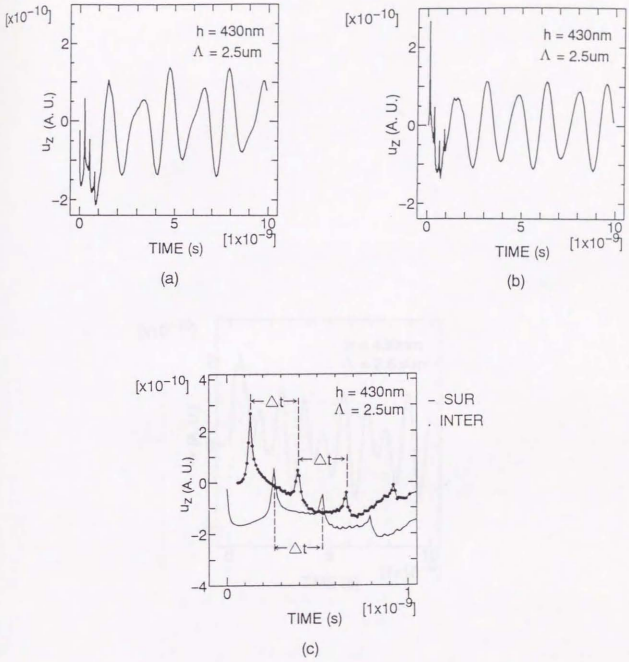

Fig. 5.4. The time responses of normal displacement amplitudes u_z at (a) the surface and (b) interface for an Au film/soda lime glass system induced by the transient grating method. (c) is a comparison of (a) and (b). The Au film thickness was 430 nm. The grating spacing was 2.5 μm.

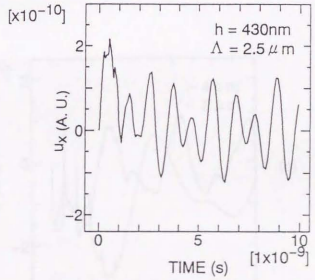

Fig. 5.5. The time responses of parallel displacement amplitudes u_x at the surface for an Au film/soda lime glass system induced by the transient grating method. The Au film thickness was 430 nm. The grating spacing was 2.5 μm.

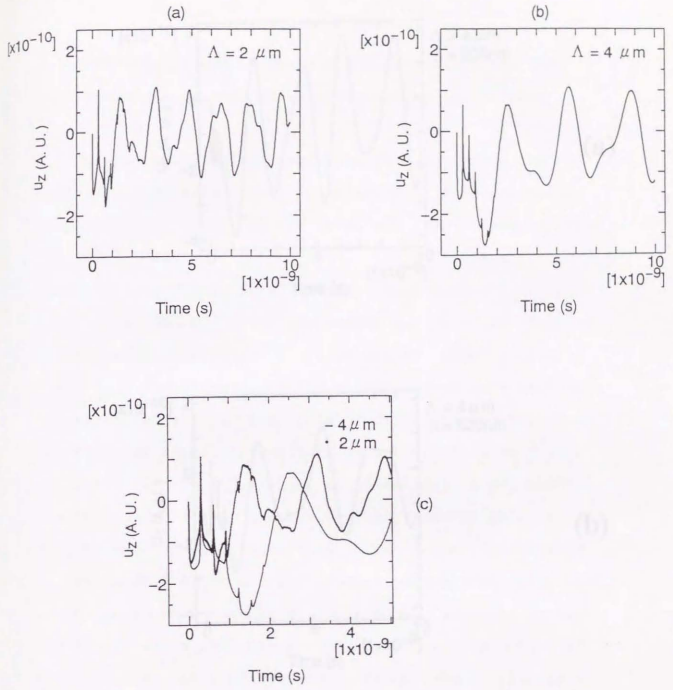

Fig. 5.6. The time responses of normal displacement amplitudes u_z at the water/Au interface for a water/Au film/soda lime glass system induced by the transient grating method. The Au film thickness was 500 nm. The grating spacings were (a) 2 and (b) 4 μm. (c) is a comparison of (a) and (b) within the time of 5 ns.

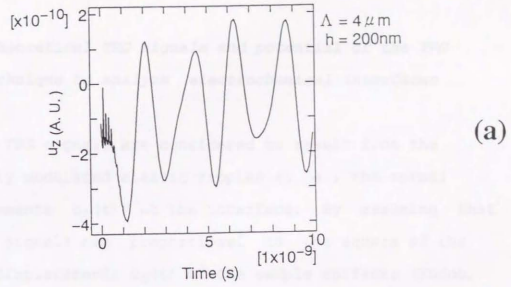

(a)

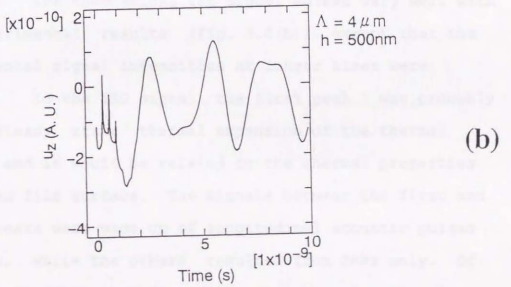

(b)

Fig. 5.7. The time responses of normal displacement amplitudes u_z at the surfaces for Au film/soda lime glass systems induced by the transient grating method. The Au film thicknesses were (a) 200 and (b) 500 nm. The grating spacing was 4 μm.

5.2.3 Theoretical TRG signals and potential of the TRG technique to analyze electrochemical interfaces

The TRG signals are considered to result from the spatially modulated elastic ripples (i. e., the normal displacements $u_z(t)$) at the interface. By assuming that the TRG signals are proportional to the square of the normal displacements $u_z(t)$ of the sample surfaces (Kudou, 1985), the TRG signal of the sample mentioned in Section 5.2.2 was calculated for a 2.5μm grating spacing (Fig. 5.8(a)). The theoretical TRG signal agreed very well with the experimental results (Fig. 5.8(b)), except that the experimental signal intensities at longer times were smaller. In the TRG signal, the first peak 1 was probably due to steady state thermal expansion of the thermal grating and it would be related to the thermal properties of the Au film surface. The signals between the first and second peaks were made up of longitudinal acoustic pulses and SAWs, while the others resulted from SAWs only. Of note was the fact that for the present sample, signals from the thermal grating were separate from those of the acoustic grating. Moreover, the two valleys B and C in the experimental result could be explained very well as longitudinal acoustic pulses, based on comparison with the theoretical result. This means that the TRG technique can be used to detect thin film thicknesses or longitudinal acoustic velocities, along with elastic and thermal

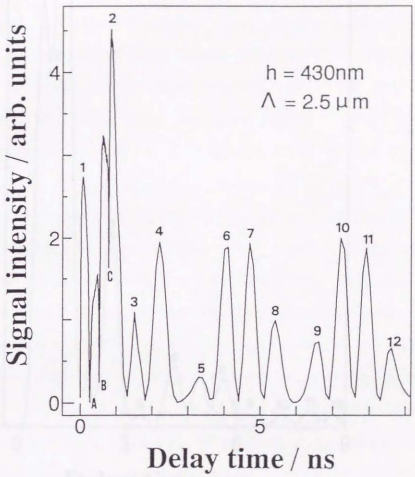
Signal intensity / arb. units
Delay time / ns
h = 430nm
Λ = 2.5 μm
0
2
4
5
1
2
3
4
5
6
7
8
9
10
11
12
A
B
C

Fig. 5.8 (a)

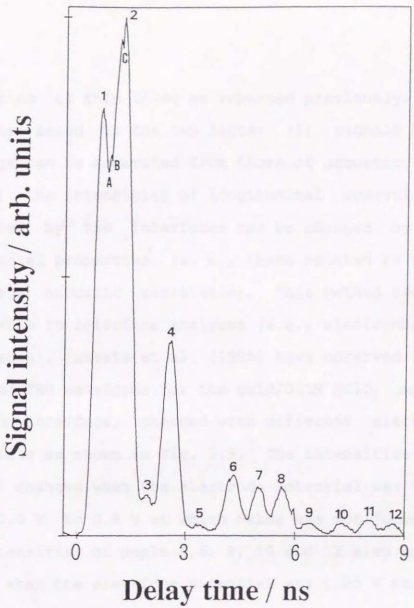

Fig. 5.8 (b)

Fig. 5.8. The TRG responses of an Au film/soda lime glass system. The Au film thickness was 430 nm. The grating spacing was 2.5 μm. (a) and (b) are theoretical and experimental results, respectively.

properties of thin films as reported previously.

Thus based on the two facts: (1) signals of thermal gratings can be separated from those of acoustic gratings and (2) the intensities of longitudinal acoustic pulses reflected by the interfaces can be changed by interfacial properties (i. e., those related to the interface acoustic resistance), this method seems applicable to interface analyses (e.g., electrochemical interfaces). Harata et al. (1995) have observed that the measured TRG waveforms for the gold/0.1M $HClO_4$ aqueous solution interface, changed with different electrode potentials as shown in Fig. 5.9. The intensities of peaks 1 and 2 changed when the electrode potential was varied from 0.0 V to 0.8 V at which oxide was not formed, and the intensities of peaks 4,6, 8, 10 and 12 also became larger when the electrode potential was 1.25 V at which oxide could be formed in the Au film. This fact indicates that some interface (double layer region) properties (such as the spatial distribution of absorbing anions) change with electrode potentials, and they can be evinced as changes of thermal and acoustic properties (such as thermal diffusivity and interface acoustic resistance) which are reflected by the changes of the TRG waveforms. This means the TRG technique is potentially useful for studying interfacial properties *in situ* which have not been well investigated because of lack of suitable measurement techniques. Quantitative analyses

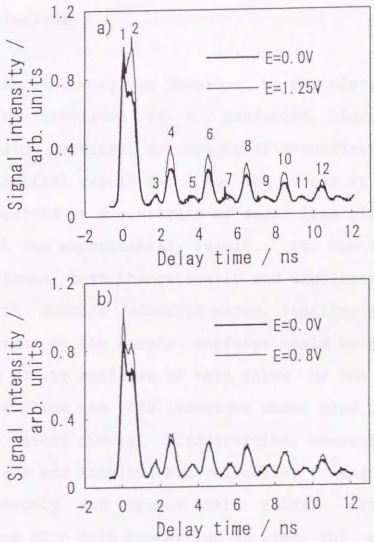

Fig. 5.9. TRG waveform dependent on electric potential. Measurement was performed for gold in 0.1M $HClO_4$ aqueous solution by setting the gold potential as 0.0, 0.8 or 1.25 V vs Ag/AgCl with Λ=1.48 μm. Numbers in Fig. (5a) are for peaks identification.

of electrode/ solution interface properties by the TRG technique remain to be studied furthermore.

5.3 Conclusions

A general theory was developed to calculate the TRG signals on interfaces (i. e., gas/solid, liquid/solid or solid/solid surfaces) for opaque film/substrate systems. The theoretical result for the TRG signal at a thin Au film deposited on a substrate of soda lime glass agreed well with the experimental result. For the first time, it was found, both theoretically and experimentally, that along with surface acoustic waves, longitudinal acoustic waves normal to the sample surfaces could be generated and detected at the surfaces of thin films by the TRG technique. Thus the TRG technique shows good potential as a way to detect thermal diffusivities, acoustic velocities (transverse and longitudinal velocities) and thicknesses simultaneously for opaque thin films. It can be used to monitor thin film properties *in situ*, for example the uniformity of a thin film or its adhesion with substrate. It was also shown that this method could be applied to analyze electrochemical interfaces *in situ*, such as changes in the properties of electric double layers versus electrode potentials.

Appendix 5.1:

In this appendix, the analytical expressions for $T_1^{(i)}(z,s)$ are derived strictly for a liquid/film/substrate system as shown in Fig. 5.1. By substituting eq. (5・4) into eq. (5・1), we can get the following equations in which $T_0^{(i)}(z,t)$ and $T_1^{(i)}(x,z,t)$ can be separated from each other

$$D_z^{(i)} \frac{\partial^2 T_0^{(i)}(z,t)}{\partial z^2} - \frac{\partial T_0^{(i)}(z,t)}{\partial t} = \begin{cases} 0, & \text{for i = 1, 3} \\ -Ae^{-\beta z}\delta(t), & \text{for i=2} \end{cases} \qquad (A・5.1)$$

$$D_z^{(i)} \frac{\partial^2 T_1^{(i)}(z,t)}{\partial z^2} - \bar{k}^2 D_x^{(i)} T_1^{(i)} - \frac{\partial T_1^{(i)}(z,t)}{\partial t} = \begin{cases} 0, & \text{for i = 1, 3} \\ -Ae^{-\beta z}\delta(t), & \text{for i=2} \end{cases} \qquad (A・5・2)$$

$T_0^{(i)}(z,t)$ and $T_1^{(i)}(x,z,t)$ can also be separated from each other in the boundary conditions as follows:

$$T_0^{(1)}(z=0) = T_0^{(2)}(z=0) \qquad k_1 \frac{\partial T_0^{(1)}}{\partial z}(z=0) = k_2 \frac{\partial T_0^{(2)}}{\partial z}(z=0),$$

$$T_0^{(2)}(z=h) = T_0^{(3)}(z=h) \qquad k_2 \frac{\partial T_0^{(2)}}{\partial z}(z=h) = k_3 \frac{\partial T_0^{(3)}}{\partial z}(z=h),$$

$$T_0^{(1)}(z \to -\infty, t) = T_0^{(3)}(z \to \infty, t) = 0, \qquad (A・5・3)$$

$$T_1^{(1)}(z=0) = T_1^{(2)}(z=0) \qquad k_1 \frac{\partial T_1^{(1)}}{\partial z}(z=0) = k_2 \frac{\partial T_1^{(2)}}{\partial z}(z=0),$$

$$T_1^{(2)}(z=h) = T_1^{(3)}(z=h) \qquad k_2 \frac{\partial T_1^{(2)}}{\partial z}(z=h) = k_3 \frac{\partial T_1^{(3)}}{\partial z}(z=h),$$

$$T_1^{(i)}(z \to -\infty, t) = T_1^{(3)}(z \to \infty, t) = 0. \qquad (A \cdot 5 \cdot 4)$$

The discussion is restricted to the determination of the periodic solution $T_1^{(i)}(x,z,t)$ only, which is important for the TRGs. First the Laplace transformation is used to reduce the partial differential eqs. (A・5・2) to ordinary differential equations:

$$T_1^{(i)}(x,z,t) \rightarrow \tilde{T}_1^{(i)}(x,z,s)$$

with

$$T_1^{(i)}(x,z,0) = 0, \quad i=1,\ 2,\ 3,$$

then

$$D_z^{(i)} \frac{\partial^2 \tilde{T}_1^{(i)}(x,z,s)}{\partial z^2} - \bar{k}^2 D_x^{(i)} \tilde{T}_1^{(i)} - s\tilde{T}_1^{(i)}(x,z,s) = \begin{cases} 0, & \text{for i = 1, 3} \\ -Ae^{-\beta z}, & \text{for i=2} \end{cases} \qquad (A \cdot 5 \cdot 5)$$

with boundary conditions:

$$\tilde{T}_1^{(1)}(0,s) = \tilde{T}_1^{(2)}(0,s) \qquad k_1 \frac{\partial \tilde{T}_1^{(1)}}{\partial z}(0,s) = k_2 \frac{\partial \tilde{T}_1^{(2)}}{\partial z}(0,s),$$

$$\tilde{T}_1^{(2)}(h,s) = \tilde{T}_1^{(3)}(h,s) \qquad k_2 \frac{\partial \tilde{T}_1^{(2)}}{\partial z}(h,s) = k_3 \frac{\partial \tilde{T}_1^{(3)}}{\partial z}(h,s),$$

$$\tilde{T}_1^{(1)}(z \to -\infty, s) = \tilde{T}_1^{(3)}(z \to \infty, s) = 0. \qquad (A \cdot 5 \cdot 6)$$

Then we solve eqs. (A・5・5) and use the boundary conditions to determine the integration constants $C_1^{(1)}(s)$, $C_1^{(2)}(s)$, $D_1^{(2)}(s)$, and $D_1^{(3)}(s)$ defined below:

$$\tilde{T}_1^{(1)}(z,s) = C_1^{(1)}(s) e^{y^{(1)} z},$$

$$\tilde{T}_1^{(2)}(z,s) = C_1^{(2)}(s) e^{y^{(2)} z} + D_1^{(2)}(s) e^{-y^{(2)} z} + M_1(s) e^{-\beta z},$$

$$\tilde{T}_1^{(3)}(z,s) = D_1^{(3)}(s) e^{-y^{(3)} z}, \qquad (A \cdot 5 \cdot 7)$$

where

$$y^{(i)} = \sqrt{\frac{s + D_z^{(i)} \bar{k}^2}{D_z^{(i)}}}, \qquad (A \cdot 5 \cdot 8)$$

$$M_1 = -A / (\beta^2 D_z^{(2)} - \bar{k}^2 D_z^{(2)} - s), \qquad (A \cdot 5 \cdot 9)$$

$$C_1^{(2)} = (N_{32}^- P_{12} - N_{12}^+ P_{32}) / (N_{12}^+ N_{32}^+ - N_{12}^- N_{32}^-), \qquad (A \cdot 5 \cdot 10)$$

$$D_1^{(2)} = (N_{12}^- P_{32} - N_{32}^+ P_{12}) / (N_{12}^+ N_{32}^+ - N_{12}^- N_{32}^-), \qquad (A \cdot 5 \cdot 11)$$

$$C_1^{(1)} = C_1^{(2)} + D_1^{(2)} + M_1, \qquad (A \cdot 5 \cdot 12)$$

$$D_1^{(3)} = C_1^{(2)} e^{(y^{(2)} + y^{(3)})h} + D_1^{(2)} e^{(y^{(3)} - y^{(2)})h} + M_1 e^{(y^{(3)} - \beta)h}, \qquad (A \cdot 5 \cdot 13)$$

$$N_{12}^{\pm} = k^{(1,2)} y^{(1)} \pm y^{(2)}, \qquad (A \cdot 5 \cdot 14)$$

$$N_{32}^{\pm} = (k^{(3,2)} y^{(3)} \pm y^{(2)}) e^{\pm y^{(2)} h}, \qquad (A \cdot 5 \cdot 15)$$

$$P_{12} = (k^{(1,2)} y^{(1)} + \beta) M_1, \qquad (A \cdot 5 \cdot 16)$$

$$P_{32} = (k^{(3,2)} y^{(3)} - \beta) M_1 e^{-\beta h}, \qquad (A \cdot 5 \cdot 17)$$

$$k^{(1,2)} = k_1 / k_2, \qquad (A \cdot 5 \cdot 18)$$

$$k^{(3,2)} = k_3 / k_2. \qquad (A \cdot 5 \cdot 19)$$

Appendix 5.2:

In this appendix, the analytical expressions for $\phi_1^{(i)}(z,s)$ and $\psi_{y1}^{(i)}(z,s)$ are derived strictly for a liquid/film/substrate system as shown in Fig. 5.1. By substituting eqs. (5・5) and (5・6) into eqs. (5・2) and (5・3), the following equations are gotten in which $\phi_0^{(i)}(z,s)$ and $\phi_1^{(i)}(z,s)$, $\psi_{y0}^{(i)}(z,s)$ and $\psi_{y1}^{(i)}(z,s)$ can be separated from each other.

$$\frac{\partial^2\phi_0^{(i)}}{\partial z^2}-\frac{1}{(v_t^{(i)})^2}\frac{\partial^2\phi_0^{(i)}}{\partial t^2}=\frac{\gamma^{(i)}}{c_{11}^{(i)}}T_0^{(i)},\qquad \text{for i=1,2 and 3}$$

$$\frac{\partial^2\psi_{y0}^{(i)}}{\partial z^2}-\frac{1}{(v_t^{(i)})^2}\frac{\partial^2\psi_{y0}^{(i)}}{\partial t^2}=0,\qquad \text{for i=2,3} \qquad (A\cdot5\cdot20)$$

$$\frac{\partial^2\phi_1^{(i)}}{\partial z^2}-\bar{k}^2\phi_1^{(i)}-\frac{1}{(v_t^{(i)})^2}\frac{\partial^2\phi_1^{(i)}}{\partial t^2}=\frac{\gamma^{(i)}}{c_{11}^{(i)}}T_1^{(i)},\qquad \text{for i=1,2 and 3}$$

$$\frac{\partial^2\psi_{y1}^{(i)}}{\partial z^2}-\bar{k}^2\psi_{y1}^{(i)}-\frac{1}{(v_t^{(i)})^2}\frac{\partial^2\psi_{y1}^{(i)}}{\partial t^2}=0.\qquad \text{for i=2,3} \qquad (A\cdot5\cdot21)$$

Since only the periodic solutions of the potentials with subscript 1 (ϕ_1 and ψ_1) are important for the TRGs, the discussion is restricted to the determination of these solutions. With the same method as that used in Appendix

5.1, the Laplace transform is done for the time variable of the above equations with the initial condition that there is no displacement or motion at t=0 and the corresponding transformed solutions are obtained as follows:

$$\tilde{\phi}_1^{(1)}(z,s) = E_1^{(1)}(s)e^{\sqrt{\bar{k}^2+s^2/(v_t^{(1)})^2}z} + \frac{r^{(1)}C_1^{(1)}/c_{11}^{(1)}}{(\gamma^{(1)})^2-[\bar{k}^2+s^2/(v_t^{(1)})^2]}e^{\gamma^{(1)}z}, \quad z<0,$$

$$\tilde{\phi}_1^{(2)}(z,s) = E_1^{(2)}(s)e^{\sqrt{\bar{k}^2+s^2/(v_t^{(2)})^2}z} + F_1^{(2)}(s)e^{-\sqrt{\bar{k}^2+s^2/(v_t^{(2)})^2}z} + \frac{r^{(2)}C_1^{(2)}/c_{11}^{(2)}}{(\gamma^{(2)})^2-[\bar{k}^2+s^2/(v_t^{(2)})^2]}e^{\gamma^{(2)}z}$$
$$+\frac{r^{(2)}D_1^{(2)}/c_{11}^{(2)}}{(\gamma^{(2)})^2-[\bar{k}^2+s^2/(v_t^{(2)})^2]}e^{-\gamma^{(2)}z} + \frac{r^{(2)}M_1/c_{11}^{(2)}}{\beta^2-[\bar{k}^2+s^2/(v_t^{(2)})^2]}e^{-\beta z}, \quad 0<z<h,$$

$$\tilde{\phi}_1^{(3)}(z,s) = F_1^{(3)}(s)e^{-\sqrt{\bar{k}^2+s^2/(v_t^{(3)})^2}z} + \frac{r^{(3)}D_1^{(3)}/c_{11}^{(3)}}{(\gamma^{(3)})^2-[\bar{k}^2+s^2/(v_t^{(3)})^2]}e^{-\gamma^{(3)}z}, \quad z>h, \quad (A\cdot 5\cdot 22)$$

$$\tilde{\psi}_{y1}^{(2)}(z,s) = G_1^{(2)}(s)e^{\sqrt{\bar{k}^2+s^2/(v_t^{(2)})^2}z} + H_1^{(2)}(s)e^{-\sqrt{\bar{k}^2+s^2/(v_t^{(2)})^2}z}, \quad 0<z<h,$$

$$\tilde{\psi}_{y1}^{(3)}(z,s) = H_1^{(3)}(s)e^{-\sqrt{\bar{k}^2+s^2/(v_t^{(3)})^2}z}, \quad z>h, \quad (A\cdot 5\cdot 23)$$

where s is the Laplace variable conjugate to time, and $v_t^{(i)}$, $v_t^{(i)}$ are the bulk longitudinal and transverse velocities in layer i (i=1, 2, and 3), respectively. The boundary conditions are as follows:

$$u_z^{(1)}(z=0) = u_z^{(2)}(z=0),$$
$$\sigma_{xz}^{(2)}(z=0) = p_L(z=0),$$
$$\sigma_{xz}^{(2)}(z=0) = 0, \qquad (A \cdot 5 \cdot 24)$$

$$u_z^{(2)}(z=h) = u_z^{(3)}(z=h),$$
$$u_x^{(2)}(z=h) = \sigma_x^{(3)}(z=h),$$
$$\sigma_{zz}^{(2)}(z=h) = \sigma_{zz}^{(3)}(z=h),$$
$$\sigma_{xz}^{(2)}(z=h) = \sigma_{xz}^{(3)}(z=h), \qquad (A \cdot 5 \cdot 25)$$

where the $u_x^{(i)}$, $u_z^{(i)}$, $\sigma_{xz}^{(i)}$, and $\sigma_{zz}^{(i)}$ are the components of the displacement vector and the stress tensor, and p_L is the pressure of the liquid.

The periodic components of the potentials with subscript 1 are also separated from those with subscript 0 in the above boundary conditions as stated in Appendix 5.1. The variables $E_1^{(1)}(s)$, $E_1^{(2)}(s)$, $F_1^{(2)}(s)$, $G_1^{(2)}(s)$, $H_1^{(2)}(s)$, and $H_1^{(3)}(s)$ are determined by imposing these boundary conditions and the relations can be conveniently expressed in matrix form as follows:

$$\mathbf{AB} = \mathbf{C}, \qquad (A \cdot 5 \cdot 26)$$

where

$$
\mathbf{A}=\begin{bmatrix}
\bar{y}_1 & -\bar{y}_2 & \bar{y}_2 & -1 & -1 & 0 & 0 \\
0 & 2\bar{y}_2 & -2\bar{y}_2 & 1+(\bar{y}_2)^2 & 1+(\bar{y}_2)^2 & 0 & 0 \\
g_1[(\bar{y}_1)^2-1] & -[1+(\bar{y}_2)^2] & -[1+(\bar{y}_2)^2] & -2\bar{y}_2 & 2\bar{y}_2 & 0 & 0 \\
0 & e^{\bar{\gamma}_2\bar{k}\bar{x}_4} & e^{-\bar{\gamma}_2\bar{k}\bar{x}_4} & \bar{y}_2 e^{\bar{\gamma}_2\bar{k}\bar{x}_4} & -\bar{y}_2 e^{-\bar{\gamma}_2\bar{k}\bar{x}_4} & -e^{-\bar{\gamma}_2\bar{k}\bar{x}_4} & \bar{y}_2 e^{-\bar{\gamma}_2\bar{k}\bar{x}_4} \\
0 & \bar{y}_2 e^{\bar{\gamma}_2\bar{k}\bar{x}_4} & -\bar{y}_2 e^{-\bar{\gamma}_2\bar{k}\bar{x}_4} & e^{\bar{\gamma}_2\bar{k}\bar{x}_4} & e^{-\bar{\gamma}_2\bar{k}\bar{x}_4} & \bar{y}_2 e^{-\bar{\gamma}_2\bar{k}\bar{x}_4} & -e^{-\bar{\gamma}_2\bar{k}\bar{x}_4} \\
0 & 2\bar{y}_2 e^{\bar{\gamma}_2\bar{k}\bar{x}_4} & -2\bar{y}_2 e^{-\bar{\gamma}_2\bar{k}\bar{x}_4} & [1+(\bar{y}_2)^2]e^{\bar{\gamma}_2\bar{k}\bar{x}_4} & [1+(\bar{y}_2)^2]e^{-\bar{\gamma}_2\bar{k}\bar{x}_4} & 2\bar{y}_2 g_2 e^{-\bar{\gamma}_2\bar{k}\bar{x}_4} & -g_2[1+(\bar{y}_2)^2]e^{-\bar{\gamma}_2\bar{k}\bar{x}_4} \\
0 & [1+(\bar{y}_2)^2]e^{\bar{\gamma}_2\bar{k}\bar{x}_4} & [1+(\bar{y}_2)^2]e^{-\bar{\gamma}_2\bar{k}\bar{x}_4} & 2\bar{y}_2 e^{\bar{\gamma}_2\bar{k}\bar{x}_4} & -2\bar{y}_2 e^{-\bar{\gamma}_2\bar{k}\bar{x}_4} & -g_2[1+(\bar{y}_2)^2]e^{-\bar{\gamma}_2\bar{k}\bar{x}_4} & 2g_2\bar{y}_2 e^{-\bar{\gamma}_2\bar{k}\bar{x}_4}
\end{bmatrix},
$$

(A・5・27)

$$
\mathbf{B}=\begin{bmatrix}
E_1^{(1)} \\ E_1^{(2)} \\ F_1^{(2)} \\ G_1^{(2)} \\ H_1^{(2)} \\ F_1^{(3)} \\ H_1^{(3)}
\end{bmatrix},
\qquad (A・5・28)
$$

$$
\mathbf{c}=\begin{bmatrix}
[\alpha_1^{(2)}y^{(2)}-\delta_1^{(2)}y^{(2)}-\beta_1\alpha_1^{(2)}-\alpha_1^{(2)}y^{(2)}]/\bar{k} \\
[-2\alpha_1^{(2)}y^{(2)}+2\delta_1^{(2)}y^{(2)}+2\beta_1\alpha_1^{(2)}]/\bar{k} \\
\{[\alpha_{11}^{(2)}(y^{(2)})^2-\alpha_{12}^{(2)}\bar{k}^2]\alpha_1^{(2)}+[\alpha_{11}^{(2)}(y^{(2)})^2-\alpha_{12}^{(2)}\bar{k}^2]\beta_1^{(2)}+[\alpha_{11}^{(2)}\beta^2-\alpha_{12}^{(2)}\bar{k}^2]\alpha_1^{(2)}+\alpha_{11}^{(2)}\alpha_{11}^{(1)}\{\bar{k}^2-(y^{(2)})^2\}+C_1^{(2)}(r^{(2)}-r^{(2)})\}/(\bar{k}^2\alpha_{11}^{(2)}) \\
[\delta_1^{(2)}e^{-r^{(2)}h}-\alpha_1^{(2)}e^{r^{(2)}h}-\delta_1^{(2)}e^{-r^{(2)}h}-\alpha_1^{(2)}e^{-\beta h}] \\
[-\delta_1^{(2)}y^{(2)}e^{-r^{(2)}h}-\alpha_1^{(2)}y^{(2)}e^{r^{(2)}h}+\delta_1^{(2)}y^{(2)}e^{-r^{(2)}h}+\beta\alpha_1^{(2)}e^{-\beta h}]/\bar{k} \\
-2[g_2\delta_1^{(2)}y^{(2)}e^{-r^{(2)}h}+\alpha_1^{(2)}y^{(2)}e^{r^{(2)}h}-\delta_1^{(2)}y^{(2)}e^{-r^{(2)}h}-\beta\alpha_1^{(2)}e^{-\beta h}]/\bar{k} \\
\{[\alpha_{11}^{(2)}(y^{(2)})^2-\alpha_{12}^{(2)}\bar{k}^2]\delta_1^{(2)}e^{-r^{(2)}h}-[\alpha_{11}^{(2)}(y^{(2)})^2-\alpha_{12}^{(2)}\bar{k}^2]\alpha_1^{(2)}e^{r^{(2)}h}-[\alpha_{11}^{(2)}(y^{(2)})^2-\alpha_{12}^{(2)}\bar{k}^2]\delta_1^{(2)}e^{-r^{(2)}h}-[\alpha_{11}^{(2)}\beta^2-\alpha_{12}^{(2)}\bar{k}^2]\alpha_1^{(2)}e^{-\beta h}+D_1^{(2)}(r^{(2)}-r^{(2)})e^{-\beta h}\}/(\bar{k}^2\alpha_{11}^{(2)})
\end{bmatrix}
$$

(A・5・29)

where

$$a_1^{(1)} = \frac{3C_1^{(1)}\alpha_T^{(1)}}{(\gamma^{(1)})^2 - (\bar{\gamma}_1 k)^2}, \qquad (A \cdot 5 \cdot 30)$$

$$a_1^{(2)} = \frac{r^{(2)}C_1^{(2)}/c_{11}^{(2)}}{(\gamma^{(2)})^2 - (\bar{\gamma}_2 k)^2}, \qquad (A \cdot 5 \cdot 31)$$

$$b_1^{(2)} = \frac{r^{(2)}D_1^{(2)}/c_{11}^{(2)}}{(\gamma^{(2)})^2 - (\bar{\gamma}_2 k)^2}, \qquad (A \cdot 5 \cdot 32)$$

$$d_1^{(2)} = \frac{r^{(2)}M_1/c_{11}^{(2)}}{\beta^2 - (\bar{\gamma}_2 k)^2}, \qquad (A \cdot 5 \cdot 33)$$

$$b_1^{(3)} = \frac{r^{(3)}D_1^{(3)}/c_{11}^{(3)}}{(\gamma^{(3)})^2 - (\bar{\gamma}_3 k)^2}, \qquad (A \cdot 5 \cdot 34)$$

$$r^{(i)} = (3c_{11}^{(i)} - 4c_{44}^{(i)})\alpha_T^{(i)}, \quad (i=2,3) \qquad (A \cdot 5 \cdot 35)$$

$$\bar{\gamma}_i = \sqrt{1 + s^2/(\bar{k}v_t^{(i)})^2}, \qquad (A \cdot 5 \cdot 36)$$

$$\bar{\gamma}_i = \sqrt{1 + s^2/(\bar{k}v_t^{(i)})^2}, \quad (i=2,\ 3) \qquad (A \cdot 5 \cdot 37)$$

$$g_1 = c_{11}^{(1)}/c_{44}^{(2)}, \qquad (A \cdot 5 \cdot 38)$$

$$g_2 = c_{44}^{(3)}/c_{44}^{(2)}. \qquad (A \cdot 5 \cdot 39)$$

Chapter 6
Conclusions and perspectives

6.1 Conclusions

In this thesis, the excellent capabilities and potentials of the transient reflecting grating (TRG) technique in studying the thermal and acoustic properties of ultrathin near-surface layers and interfaces have been demonstrated, experimentally and theoretically. The advantages of the TRG technique over many other conventional methods can be summarized as follows.

(1) It can be used *in situ* to detect thermal and acoustic properties, and film thicknesses, **at the same time**, in a non-contact, non-destructive way, which is almost impossible by traditional techniques.

(2) It has a high degree of temporal resolution up to a few dozen ns and spatial resolution up to a few dozen nm in depth, so it can be used to study ultrafast photothermal (PT) and photoacoustic (PA) phenomena which are rather difficult to elucidate by conventional PT and PA methods.

(3) It is very sensitive and selective to the properties of surfaces or interfaces within a region of a few dozen nm to a few hundred nm in depth.

(4) It can be used effectively even under such severe

conditions as low and high temperatures, and high pressure, and when samples are contained in liquids.
(5) It can be used for generating and detecting high-power coherent SAWs or interfacial waves of a few MHz to 30GHz on the sample surfaces or interfaces, even if samples are nonpiezoelectric.

The TRG technique was applied to investigate the properties of interesting sample systems such as ultrathin DLC coatings, metallic multilayered films and solid-liquid interfaces, by which its outstanding capabilities were demonstrated. The results can be summarized as follows:

(1) The TRG technique was used to evaluate the thermal properties of ultrathin DLC film (thickness: 40nm) on multilayered substrate. The result proved the potential of the TRG method in determining thermal properties of a near-surface layer as thin as a few dozen nm.
(2) The TRG technique was also used to characterize ion-implanted DLC coatings. It was observed that the waveforms of the TRG responses varied with the changes of ion implantation doses. Moreover, it was found that the DLC film with a higher ion implantation dose became hardened relative to a nonimplanted sample. These findings indicated that the TRG responses can be used to monitor the changes of properties and structures of DLC films due to different ion implantation doses.

(3) A method was developed theoretically and experimentally to detect the elastic properties of intermediate layers besides surface layers for ultrathin multilayered films using the TRG technique. The method was demonstrated by measuring the acoustic velocities of the Au layer (thickness: 300nm) and the Cr layer (thickness: 30nm) for a Au/Cr/quartz sample. Results obtained from this method can be used to provide important information about the mechanical and adhesive properties of multilayer systems, especially for the intermediate layer.

(4) A general theory to analyze the TRG signals of interfaces (e. g., gas/solid, liquid/solid etc.), especially for liquid/film/solid systems, was developed. Experimental results could be well explained using this theory. For the first time, it was found in theory and experiment that longitudinal acoustic pulses (frequency: from a few tens of GHz to a few hundred GHz) normal to the sample surface could be generated and detected at the surfaces of thin films by the TRG technique. The capabilities and potentials of the TRG technique to evaluate the properties of liquid/solid interfaces *in situ* such as electrode/solution interfaces were discussed. It was proposed that this method can be applied to analyze electrochemical interfaces *in situ*, such as changes in the properties of electric double layers versus electrode potentials.

6.2 Perspectives

On the basis of these results and discussions, some perspectives of the TRG technique can be given. First, the results of thermal and acoustic properties of ultrathin films on substrates determined by the TRG technique can give important information about their purity, homogeneity, microstructure, and adhesion to the substrates. So the TRG technique can be applied to monitor film properties and quality during and after fabrication as an *in situ*, non-contact, non-destructive method. Second, the TRG signal measured at different grating spacing is selectively sensitive to the thermal and acoustic properties of different depths. Thus, depth profiling of the thermal and acoustic properties of samples, such as the ion-implanted DLC films, is also possible by analyzing the TRG responses with a variety of grating spacings. Third, due to the fact that the reflectivity of the longitudinal acoustic echoes generated at the sample surface for a liquid/film /solid system by the TRG method is related to the properties of the liquid/film interface, such as the density and acoustic velocity etc., the electrochemical interface can be characterized by measuring these echoes. By using a ultrafast pulse laser with a pulse width of a few hundred femtoseconds, the ultrafast change of the properties of the electrode/solution interface such as the

electric double layer with varying electrode potentials, can be studied by measuring the reflectivity of the echoes which appear almost within the first 1 ns after excitation.

Acknowledgments

I would like to express my greatest appreciation to my supervisor Professor Tsuguo Sawada, for his patient guidance, instruction, and encouragement throughout my study. I am very grateful to Prof. Sawada for all the help he has so kindly offered.

I would like to deeply thank associate Professor Takehiko Kitamori, for his helpful advice, instructive comments and discussions.

I would like to express my sincere appreciation to Dr. Akira Harata, for his constant help, useful comments and instructive advice and discussions, which gave me deeper understanding of the TRG technique.

I am also deeply grateful to Dr. T. Odake, Dr. S.Takahasi, Mr. T. Tanaka, Mr. T. Shimosaka, Miss G. H. Yin, Mr. M. Kawanishi, Mr. N. Adachi, Mr. T. Edo, and all other members of Prof. Sawada's Laboratory for their useful help and hearty kindness, which give me a comfortable and active environment for pursuing my studies.

I would like to acknowledgment the financial support of the Japan Society for the Promotion of Science.

I am very grateful to Prof. Shu-yi Zhang, Institute of Acoustics, Nanjing University, China, for her patient guidance before I came to Japan. Without the foundation she provided, I would not have been able to continue my studies here.

Finally, I say thank you to my parents, brothers, and all of my friends for their continuous encouragement and friendship. They have given me a lot of self-confidence, especially when I had difficulties in my studies or my life.

Publications List

(1) Q. Shen, A. Harata and T. Sawada, Jpn. J. Appl. Phys. Vol.**32** (1993) pp. 3628.
Analysis of Metallic Multilayers Using Hypersonic Surface Waves Induced by Transient Reflecting Gratings

(2) Q. Shen, A. Harata and T. Sawada, J. de Physique, Vol. **4** (Paris, 1994), C7-233.
Analysis of Ion Implanted Diamond-Like-Carbon Films Using Laser-Induced Transient Reflecting Grating Technique

(3) Q. Shen, A. Harata and T. Sawada, J. Appl. Phys., Vol. **77** (1995) in press.
Analysis of the Thermal and Acoustic Properties of Ion-Implanted Diamondlike Carbon Films Using the Transient Reflecting Grating Technique

(4) Q. Shen, T. Edo, A. Harata and T. Sawada, in preparation.
Analysis of Thin Films and Electrode/Solution Interfaces by Transient Reflecting Grating Technique

(5) Harata, A., Shen, Q., Tanaka, T., and Sawada, T., Jpn. J. Appl. Phys., Vol. **32** (1993) 3633.
Laser-Stimulated scattering microscope study of an ion-implanted silicon surface.

(6) Harata, A., Nishimura, H., Shen, Q., Tanaka, T., and Sawada, T., J. de Physique, Vol. **4** (Paris, 1994), C7-159.
Transient reflecting grating study of ion-implanted semiconductor

References

Auth, D. C., Appl. Phys. Lett. **16**(12), 521 (1970)

Blech, I. A. and Wood, P., J. Vac. Sci. Technol. A **11**, 728 (1993).

Bloembergen, N., Bret, G., Lallemand, P., and Sinowa, A. S. P., IEEE J. QE **3**, 197 (1967).

Boersch, H., Eichler, H. J., Z. Angew. Phys. **22**, 378 (1967).

Briggs, A., *An Introduction to Scanning Acoustic Microscopy*, (Oxford University Press, New York, 1985).

Cachier, G., Appl. Phys. Lett. **17**, 419 (1970).

Chronological Scientific Tables, ed. National Astronomical Observatory of Japan (Maruzen, Tokyo, 1990) p.494.

Clemens, B. M. and esley, G. L., Phys. Rev. Lett. **61**, 2356 (1988).

Danner, R., Huebener, R. P., Chun, C. S. L., Grimsditch M., and Schuller, I. K., Phys. Rev. B **33**, 3696 (1986).

Dearnaley, G., Freeman, J. H., Nelson, R. S., and Stephen, J., *Ion Implantation* (North-Holland, Amsterdam, 1973) p. 766.

Denariez, M., and Ret, G., Phys. Rev. **171**, 1601 (1968)

Doyama, M. and Yamamoto, R., Eds., *Processing Techniques of Materials* (Academic, Tokyo, 1987) p. 231 (in Japanese).

Duggal, A. R., Rogers, J. A., and Nelson, K. A., Appl. Phys. Lett. **60**, 692 (1992a).

Duggal, A. R., Rogers, J. A., and Nelson, K. A.,

J. Appl. Phys. **72**, 2823 (1992b).

Eichler, H., Enterlein, G., Munschau, J., Stahl, H., Angew. Phys. **31**, 1 (1971).

Eichler, H. J., Gunter, P. and Pohl, D. W., *Laser-Induced Dynamic Gratings*, ed. T. Tamir (Spring-Verlag, Berlin, 1986) Vol. **50**, Chap. 1.

Eichler, H., Salje, G., Stahl, H., J. Appl. Phys. **44**, 5383 (1973)

Eichler, H., Stahl, H., J. Appl. Phys. **44**, 3429 (1973)

Faran, K. J., Miller, R. J. D., and Gracewski, S. M. J., Appl. Mechanics **57**, 415 (1990).

Farnell, G. W., in *Physical Acoustics*, eds. Mason, M. P. and Thurston, R. N. (Academic, New York, 1969) Vol. **6**, p. 109.

Farnell, G. W. and Adler, E. L., in *Physical Acoustics*, eds. Mason, M. P. and Thurston, R. N. (Academic, New York, 1972) Vol. **9**, p. 35.

Fayer, M. D., IEEE J. Quantum Electron. QE-**22**, 1437 (1986).

Fishman, I. M., Marshall, C. D.,Meth, J. S., and Fayer, M. D., J. Opt. Soc. Am. B **8**, 1880 (1991).

Fishman, I. M., Marshall, C. D., Tokmakoff, A. and Fayer, M. D., J. Opt. Soc. Am. B **10**, 1006 (1993).

Grahn, H. T., Maris, H. J., and Tauc, J., IEEE J. Quantum Electro. QE-**25**, 2562 (1989).

Gray, D. E., Ed., *American Institute of Physics Handbook*, 3rd ed. (McGraw-Hill, New York, 1972), p. 6-132.

Grudzinskaya, I. S., and Pyatakov, P. A., Sov. Phys. Acoust.

35, 356 (1989).

Harata, A., Ph. D. Thesis, University of Tokyo (1990).

Harata, A., in *Kagaku to Kogyo* (Chemistry and Chemical Industry, Chem. Soc. Jap) **45**, 229 (1992) (in Japanese).

Harata, A., Kawasaki, T., Ito, M., and Sawada, T., Anal. Chim. Acta. **299**, 349 (1995).

Harata, A., Nishimura, H., and Sawada, T., Appl. Phys. Lett. **57**, 132 (1990).

Harata, A., Nishimura, H., Tanaka, T., and Sawada, T., Rev. Sci. Instrum. **64**, 618 (1993a).

Harata, A., Sawada, T., Jpn. J. Appl. Phys. Suppl. **27**, 223 (1988).

Harata, A., Sawada, T., Appl. Phys. Lett. **58**, 1839 (1991).

Harata, A., Sawada, T., Gohshi, Y., Jpn. J. Appl. Phys. Suppl. **26**, 41(1987).

Harata, A., Shen, Q., Tanaka, T., and Sawada, T., Jpn. J. Appl. Phys. **32**, 3633 (1993b).

Hosono, T., *Fast Laplace Transformations with Basic*, (Kyouritu Publication, Tokyo, 1984) p. 17 (in Japanese).

Jackson, W. B., et al., Appl. Opt. **20**, 1333 (1981).

Jáuregui, J. and Matthias, E., Appl. Phys. A **54**, 35 (1992).

Käding, O. W., Matthias, E., Zachai, R., Fusser, H.-J., and Munzinger, P., Diamond and Related Mater. **2**, 1185 (1993).

Karner, C., et al., Appl. Phys. A 38, 19 (1985)

Kasinski, J. J., Gomez-Jahn, L., Leong, K. J., Gracewski,

S. M., and Miller, R. J. D., Opt. Lett., Vol. **13**, 710 (1988).

Kodou K. E., *Basis and Method of Spectroscopy* , (Ohmu Corporation, Tokyo, 1985), p.372.

Kolsky, H., Ed., *Stress Waves in Solids* (Dover Publications, Inc., New York, 1963) p. 7.

Kuo, P. K., Favro, L. D., and Thomas, R. L., in *photothermal investigation of solids and fluids*, ed. Sell, J. A., (Academic Prees, New York, 1989), p. 191.

Kuo, P. K., Wei, L., and Thomas, R. L., Conference Digest and Technical Abstracts of the 7th International Topical Meeting on Photoacoustic and Photothermal Phenomena (Doorwerth, The Netherlands, 1991), p.465.

Kushibiki, J. I. and Chubachi, N., IEEE Trans. Sonics & Ultras. SU-**32**, 189 (1985).

Lai, H. M., et al., J. Acoust. Soc. Am. **72**, 2000 (1982).

Lettington, A. H., Phil. Trans. R. Soc. Lond. A. **342**, 287 (1993).

Marchon, B., Heiman, N. M. R., Lautie, K. A., Ager III, J. W., and Veirs, D. K. J., Appl. Phys. **69**, 5748 (1991).

Marshall, C. D., Fishman, I. M., Dorfman, R. C., Eom, C. B., and Fayer, M. D., Phys. Rev. B **45**, 10009 (1992).

Miller, R. J. D., Casalegno, R., Nelson, K. A., and Fayer, M. D., Chem. Phys.**72**, 371 (1982).

Miller, R. J. D., Pierre, M., Rose, T. S., and Fayer, M. D., J. Phys. Chem. **88**, 3021 (1984).

Nakaue, H., Mitani, T., Kurokawa, H., Yonezawa, T., and Yoshio, H., Thin Solid Films **212**, 240 (1992).

Nakayama, Y., Gomi, Y., and Okada, T., J. Appl. Phys. **61**, 5012 (1987).

Nelson, K. A., Miller, R. J. D., Lutz, D. R., and Fayer, M. D., J. Appl. Phys. **53**, 1144 (1982).

Nishimura, H., Harata, A., and Sawada, T., Jpn. J. Appl. Phys. **32**, 5149 (1993).

Nowacki, W., *Thermoelasticity* (Pergamon, New York, 1986).

Olmstead, M. A., et al., Appl. Phys. A **32**, 141 (1983).

Petzoldt, S., et al., Appl. Phys. Lett. 53, 2005 (1988).

Phillion, D. W., Kvizerga, D. J., Siegman, A. E., Appl. Phys. Lett. **27**, 85 (1975).

Pohl, D. W., Phys. Rev. Lett. **23**, 711 (1969).

Pohl, D. W., Maier, M., and Kaiser, W., Phys. Rev. Lett. **20**, 366 (1968a).

Pohl, D. W., Reinhold, I., and Kaiser, W., Phys. Rev. Lett. **20**, 1461 (1968b).

Robertson, J., Surface and Coatings Technology **50**, 185 (1992).

Rogers, J. A., Dhar, L., and Nelson, K. A., Appl. Phys. Lett. **65**, 312 (1994).

Rogers, J. A. and Nelson, K. A., J. Appl. Phys. **75**, 1534 (1994).

Rosencwaig, A., et al., Appl. Phys. Lett. **46**, 1013 (1985).

Rother, W., Pohl, D. W., and Kaiser, W., Phys. Rev. Lett. **22**, 915 (1969).

Sandercock, J. R., Solid State Commun. **26**, 547 (1978).

Savvides, N. and Bell, T. J., J. Appl. Phys. **72**, 2791 (1992).

Savvides, N. and Bell, T. J., Thin Solid Films **228**, 289 (1993).

Schramm, K. H., Z. Metallk. **53**, 729 (1962).

Shen, Q., Harata, A., and Sawada, T., Jpn. J. Appl. Phys. **32**, 3628 (1993)

Shen, Q., Harata, A., and Sawada, T., J. de Physique (Paris) **4**, C7-233 (1994).

Shen, Q., Harata, A., and Sawada, T., J. Appl. Phys. **77**, in press (1995a).

Shen, Q., Harata, A., and Sawada, T., in preparation, (1995b).

Thomsen, C., Grahn, H. T., Maris, H. J., and Tauc, J., Phys Rev. B **34**, 4129 (1986).

Welsch., E., et al., J. Appl. Phys. **67**, 6575 (1990).

Wright, O. B., Matsumoto, T., Hyoguchi, T., and Kawashima, K., in *Physical Acoustics*, eds. Leroy, O. and Breazeale, M. A., (Plenum, New York, 1991) p. 659.

Wu, R. L. C., Surface and Coatings Technology **51**, 258 (1992).

Yan, Y.-X., Cheng, L.-T., and Nelson, K. A., J. Chem. Phys. **88**, 6477 (1988).

Yamamoto, T., Surface Technology **44**, 790 (1993).

Symbols

α_T: Coefficient of linear volume expansion

β : Optical absorption density

c_{ij} : Elastic constant

C_s : Heat capacity per unit mass at constant strain

D_i : Thermal diffusivity along i direction

$E^{(\epsilon,\Lambda)}$: Effective Young's modulus

F : SAW frequency

fi: Frequency of Rayleigh-Like mode i

$\delta(t)$: δ-Function

ϕ : Longitudinal potential of displacement **u**

ψ : Transverse potential of displacement **u**

γ : $\gamma = (3c_{11} - 4c_{44})\alpha_T$

h_{th} : Thermal penetration depth

I : Optical intensity

$\bar{k}$: Acoustic wave number

k : Acoustic wave vector

k_{eff} : Effective lateral thermal diffusivity

k_l : Lateral thermal diffusivity

k_{th} : Thermal conductivity

k_v : Vertical thermal diffusivity

λ : Wavelength of the excitation pulses

Λ : Grating spacing

θ : Half of the crossing angle of the two excitation pulses

Q : Absorbed heat per unit time per unit volume

R : Optical reflectivity

ρ : Density

s : Complex frequency in Laplace transforms

σ_{ij} : Stress tensor component

$\sigma^{(\epsilon,\Lambda)}$: Poisson's ratio

T : Temperature

$\tilde{T}(s)$: Laplace transform of temperature T(t)

τ_A : Attenuation time constant for SAW

τ_t : Attenuation time constant for temperature

u : Displacement

v_l : Longitudinal wave velocity

v_R : SAW velocity

v_t : Shear wave velocity

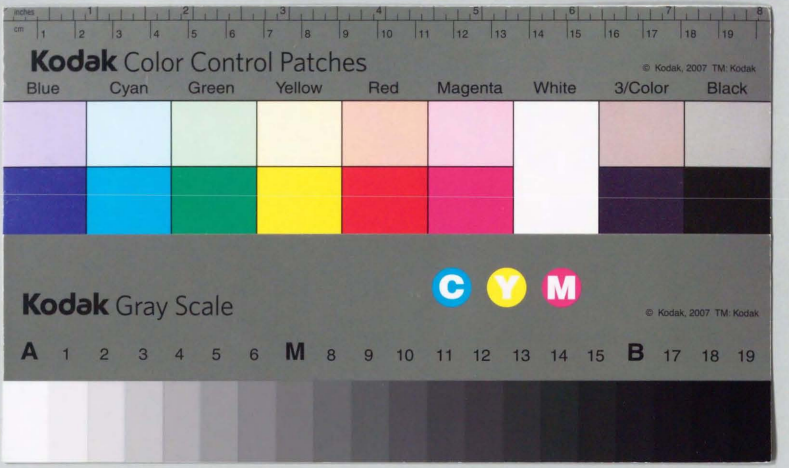
inches
cm
Kodak Color Control Patches
© Kodak, 2007 TM: Kodak
Blue
Cyan
Green
Yellow
Red
Magenta
White
3/Color
Black
Kodak Gray Scale
C
Y
M
© Kodak, 2007 TM: Kodak
A 1 2 3 4 5 6 M 8 9 10 11 12 13 14 15 B 17 18 19